Iranian Journal of Astronomy and Astrophysics
Vol. 10, No. 1, Winter 2023, 11–60
©Available online at http://ijaa.du.ac.ir
DOI: 10.22128/ijaa.2023.673.1145
Online ISSN: 2383–403X

Iranian Journal of Astronomy and Astrophysics

Review Paper

Review of Fast Solar Jets and Coronal Mass Ejections

Sima Zeighami*[1] · Ehsan Tavabi[2]

[1] Department of Physics, Tabriz Branch, Islamic Azad University, Tabriz, Iran;
*email: zeighami@iaut.ac.ir

[2] Physics Department, Payame Noor University (PNU), 19395-3697-Tehran, I. R. of Iran;
email: e_tavabi@pnu.ac.ir

Received: 13 April 2023; **Accepted:** 13 September 2023; **Published:** 30 September 2023

Abstract.

The Sun is a magnetically active star. It has a powerful magnetic field that shifts slightly from year to year until it reverses about every eleven years. The sun's magnetic field has many effects, the collection of which is called solar activity such as, sunspots, solar flares, and coronal mass ejections (CMEs). Currently, it is only possible to predict a magnetic storm 30 to 60 minutes before it occurs, which is a very short time. Solar flares and CMEs, massive eruptions of superheated plasma, are the two most energetic phenomenon which impulsively ejected and accelerated by releasing magnetic energy in the solar corona. Heliosphere, space weather, and the Earth are affected from transporting coronal plasma. Following the occurrence of these phenomenon in the Sun, the solar wind blows with greater speed and intensity and sends energetic charged particles into the space of the solar system. When these particles reach the Earth, their radiating electromagnetic waves interact with magnetic field of the Earth. Then various effects are observed, as shock waves and massive geomagnetic storms that disrupt satellites and power grids. Today, using the advancements of ground and space technology, the solar surface can be easily observed. Therefore, observation and prediction of solar storm will be possible more than in the past. In this paper, we review papers intended to collect comprehensive information about what has already been researched about fast solar jets and CMEs made by ground and space instruments over the last decades.

Keywords: Solar Jets, Bright Points, CMEs, Chromosphere, Transition Region, Corona

1 Chromospheric Spicules

Spicules manifest as slender, filamentous formations, stretching from the chromosphere into the corona as gaseous outbursts [69]. [65] determined spicule dimensions as about 3 arcsec width and 12 arcsec height from the Northwestern Observatory spicules program. The existence of Ca II emission within spicules hints at the potential existence of cooler regions caused by temperature variations perpendicular to the spicule axes [13]. In the [72], it was established that the average upward velocities of spicules were approximately 32 km s^{-1}. Interestingly, there were instances of apparent downward movements, which exhibited a

* *Corresponding author*

loose correlation with the upward velocities [72]. [23] found that the line-of-sight velocities of some spicules reverse in direction.

Spicules arise from supergranule borders. Ly-α brightness of these regions has some ten times the Sun brightness [14]. [14] suggested that in the network areas the radiation pressure gradient is comparable to that due to gravitation. [121] studied spectral Observations of solar chromospheric spicules. They pointed out that as the height increases, all prominent spectral lines, such as H and K, transition from self-reversed or flat-topped shapes to Gaussian profiles. However, the D2 line exhibits a Gaussian profile with a widening half-width as altitude increases. [67] determined line-of-sight velocity of chromospheric spicules as about 23 kms^{-1} tending to increase with height. Furthermore, they discovered that the propagation velocity surpasses 300 km s^{-1}. [42] illustrated the process which is known damping the Alfven waves. In reference to [25], it is demonstrated that spicules can have a substantial impact on maintaining the energy equilibrium and heating processes within the upper layers of the solar atmosphere. [13] studied broadening of Ca II Line Profiles in Chromospheric spicules, and found an additional motion of the ions. This may be due to an interaction between magnetic lines of force and spicule velocity. In [33], it was determined that chromospheric jets are observable within the interiors of supergranular cells, specifically in regions where the intensities of chromospheric and transition zone spectral lines are relatively low. Spicules manifest as dynamic spikes within the solar corona due to a discrepancy in density between the chromospheric material and the material composing the solar corona [120], [1], [3], [85], [32], [88], and [105]. Spicules hover above the borders of chromospheric cells, and their length varies from a few million meters to over 10 Mm. The researchers in [86] have observed that the origins of spicules align with areas of increased brightness in the Ca II H line filter on the solar surface. Variations in spicules along the solar limb can be detected through both visual and spectral means. Visual observations reveal variations in the intensity of spicules and apparent shifts in their axes. The significance of such observations has increased notably following the deployment of the Solar Optical Telescope (SOT) on the *Hinode* spacecraft. This telescope, installed on the spacecraft, has enabled the study of these fluctuations with a high degree of spatial and temporal precision. [89] studied solar limb and disk spicules and detected spicules oscillations. They also analyzed overlaps effects of spicules by simulation model assuming different positions of limb and disk spicules. Additionally, they examined a predefined selection of spicules characterized by varying heights, lifespans, and tilt angles. They conducted simulations and subsequently analyzed the outcomes, considering three distinct spatial resolutions of the frames and varying spicule number densities. They obtained the exact period of the spicule by using the wavelet method. They compared their findings with chromospheric observations conducted by Coronal Explorer (TRACE) filtergrams (1600Å), Sac-Peak Dunn's VTT (Hα), and *Hinode* (Ca II H). Their results suggested that the apparent oscillations seen in the spicules are significantly affected by overlapping effects.

Space observations with a high degree of resolution provide detailed data about the formation dynamics and origin of spicules. High-frequency oscillations of magneto-acoustic waves in spicules due to Photospheric granular forcing have been reported [117]. The oscillation period of kink waves within a magnetic cylinder placed in a field-free environment was ascertained using the MHD seismology technique [2], [4]. Authors in [88] by 1-D Fourier transformation at different heights above the solar limb showed for the first time, from 0.18 to 0.25 Mm. They can be related to the type II spicules. Spicules have transverse periodic fluctuations [88]. They obtained the x-t diagram for different heights (see Figures 1-3).

[94] analyzed observations of a quiet solar region by using *Hinode* in Ca II H in November 2006 (Figure 4). Madmax operator was used to reduce noise and improve the image of spicules. They studied the relation between off-limb and on-disk spicules (Figure 5). They

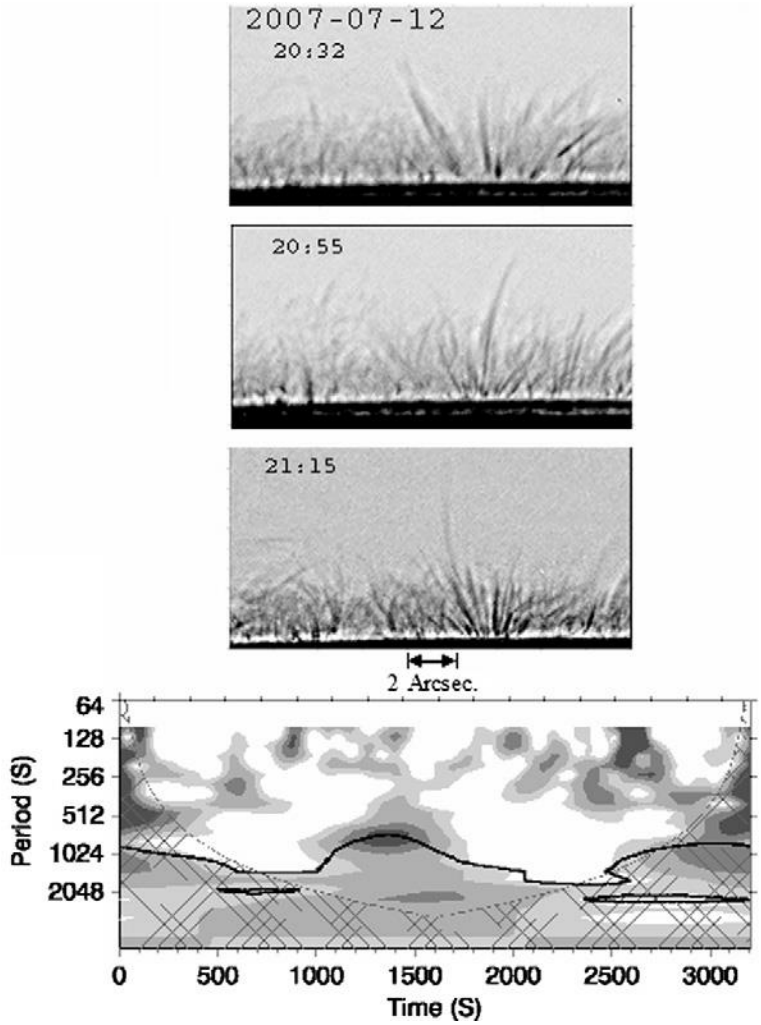

Figure 1: Ca II H (3968Å) spicules, from 19:00 to 22:00 UT on 12 July 2007, centered at position X = 610, Y = 710 arcsec in the heliocentric coordinate, and the wavelet power [89].

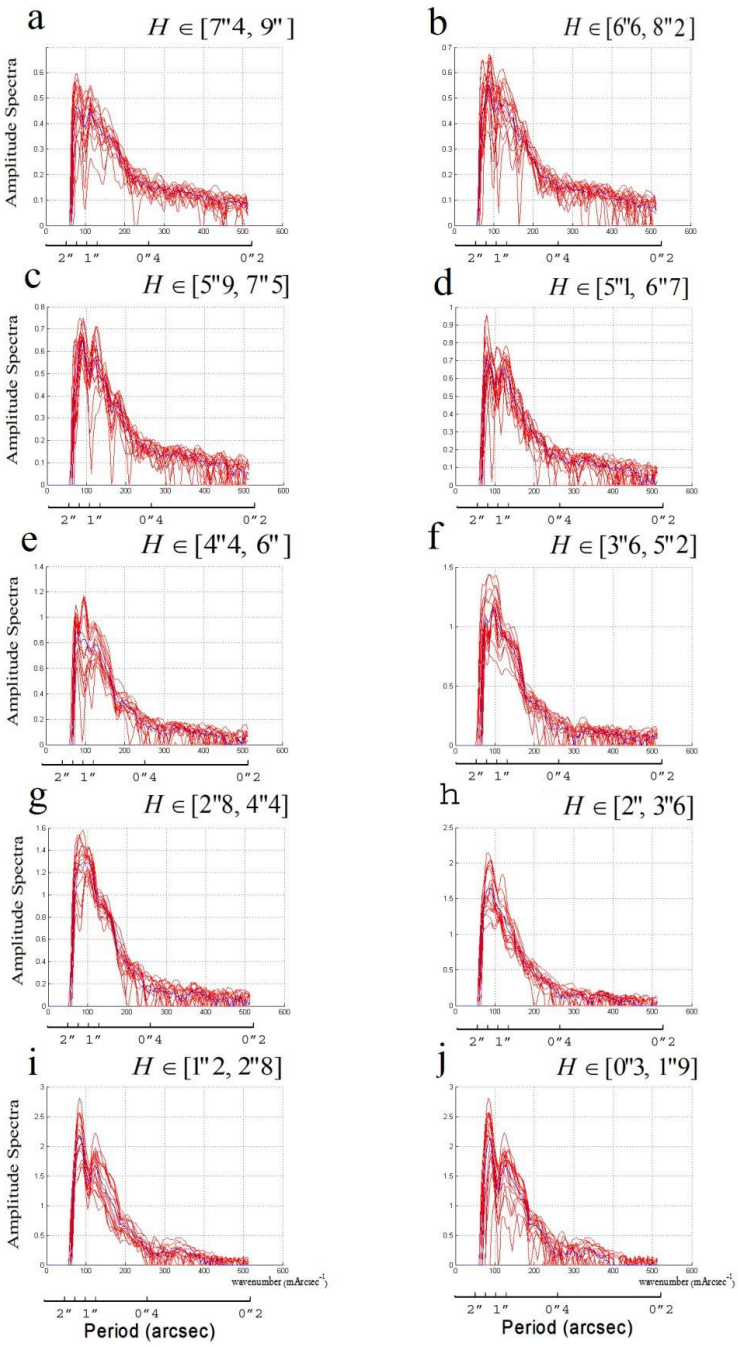

Figure 2: Fourier transformations of time series [88].

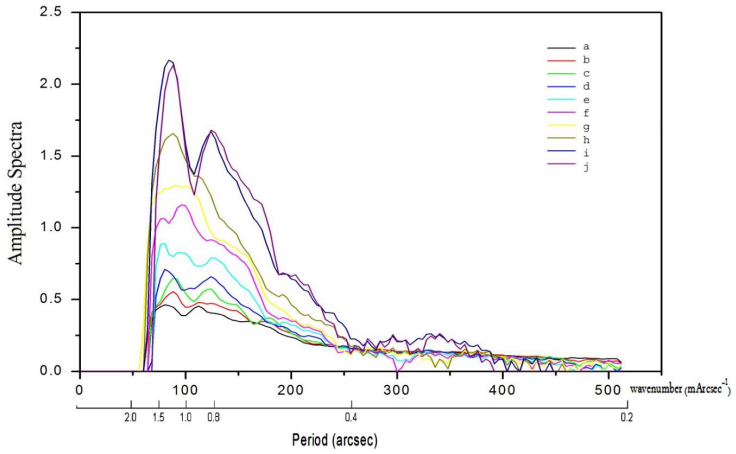

Figure 3: Time average of amplitude spectra for different heights above the solar limb [88].

showed a strong correlation between the limb and near-limb fast jets. They presented 1-D Fourier power spectra obtained at various locations on the solar disk and above its limb. They detected fluctuations with 3 min and 5 min, and less than 100 s. Researchers in [90] investigated the orientation of the EUV jets in the different solar latitudes. They used Ca II H data from the SOT/*Hinode* mission, and determined the orientations of jets by applying the Hough transform from the polar to the equator regions (Figure 6). As one moves from the solar equator towards the poles, the inclination angle of the spicules decreases, and their apparent length increases. As a result, it can be said that the chromosphere is thicker in this state compared to the maximum solar activity. In the event that spicules within the polar coronal holes exhibit a substantial increase in inclination angle, the thickness of the chromosphere and even the transition region would decrease. Conversely, large-scale activities with brief lifespans do not have a notable impact on chromospheric thickness and are effectively filtered out when averaging over extended measurement periods. During periods of minimum solar activity, the largest statistical concentration of spicules is observed in polar regions and lower latitudes, primarily consisting of spicules with more significant inclination angles. Conversely, in the peak phase of the solar cycle, the reverse trend is anticipated, which offers a topological explanation for the expansion of the chromosphere during periods of minimal solar activity.

A behavior surge-like has been seen on many of the solar limb spicules. Therefore a multi-component behavior with twisted threads is supported. In reference to [93] an examination was conducted on the equivalent of limb spicules when observed on the solar disk. The study demonstrated that the lateral movement of spicules beyond the solar limb could be influenced by the rotational motion occurring at the base of spicules on the solar disk, as depicted in Figure 7. They obtained Movements of the luminous points along the perimeters of the network in the range of 200 to 400 km, indicating vortex motion. Their results confirm splitting process and showed the existence of multi-threaded spicules. They proposed this mechanism in the context of doublet or multi-component spicules. The initiation of Alfvenic wave propagation within the spicules can be attributed to mode propagation, aligning with recent findings highlighting the existence of multiple structures within spicules. It can not be detected the spinning spicules from the disk Dopplergram observations. They generated 3D time-slice diagrams represented as columns, with axes along

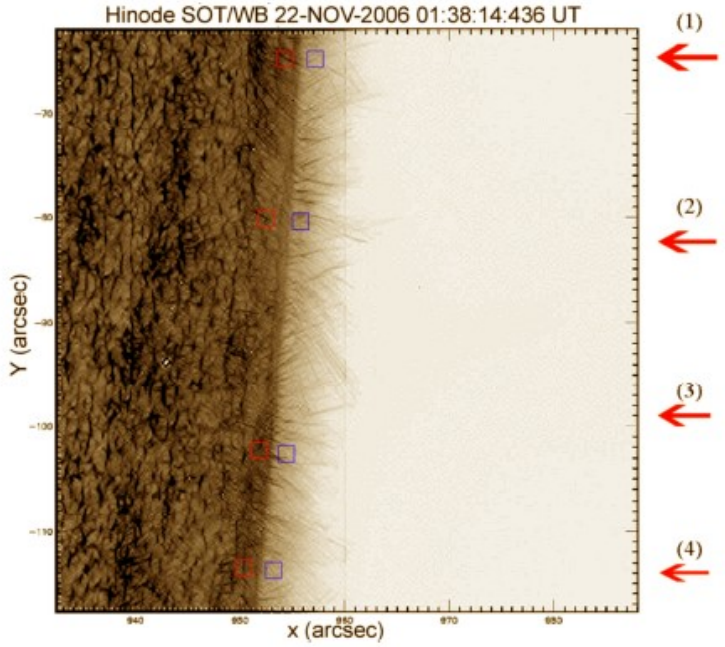

Figure 4: Applying Madmax operator on SOT (*Hinode*) images [94].

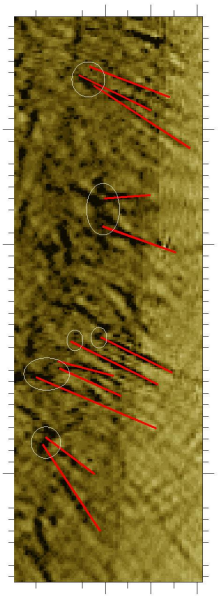

Figure 5: Negative of Figure 4 showing spicules and bright points [94].

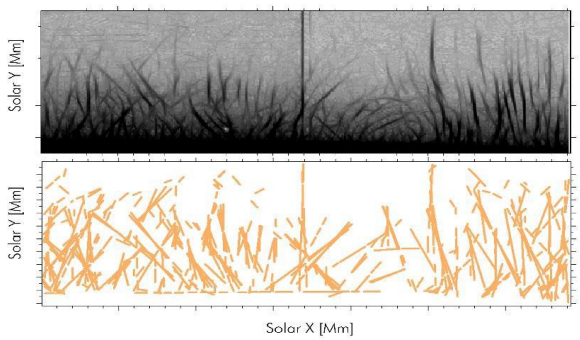

Figure 6: From top to Bottom, processed image and applying the Hough transform [90].

the x, y, and time on the z-axis. These diagrams involved successive, partially transparent slices arranged in perspective, allowing the visualization of rotational patterns within the chromospheric rosettes. These representations offered valuable insights into spinning motion, helical wave propagation, and splitting phenomena, as depicted in Figures 8 and 9. In a previous study by [17], they documented the existence of minute cellular structures that appear as bright, circular formations beneath dark mottles. These structures, referred to as rosettes, typically exhibit a circular shape and are characterized by their brightness in the chromosphere. Remarkably, rosettes undergo rapid deformation during their lifetime and can even disintegrate into smaller, distinct bright points. The phenomenon of splitting, as observed in the form of doublet spicules, has been documented by researchers in reference [87]. Recently [88] reported this behavior as multi-component spicules. [86] described in detail for limb spicules with SOT/*Hinode* instrument using highly processed data at best available spatial resolution. The existence of spectral features exhibiting an inclination relative to the dispersion direction has been attributed to the rotational motion of spicules. This value is about 25-30 km s^{-1}, like the swaying motion,15-20 km s^{-1}, [31], [88].

The dynamic characteristics of an incompressible magnetic fluid with an X-shape was investigated by [92]. This incident took place during the process of magnetic reconnection within the region responsible for jet formation. The researchers took into account the impact of viscosity in the context of closed line-tied magnetic X-shaped nulls and discovered a correlation with observations made by *Hinode*. Specifically, they found concurrence between the oscillatory and non-oscillatory behaviors of solar jets observed in the chromosphere and the corona. These findings indicated that the influence of viscosity played a significant role in the magnetic reconnection process, contributing to oscillations within the cool solar jet group observed in the Ca II H line.

[97] illustrated that the rate of upward motion was slightly higher at high levels. Their research revealed that a substantial number of spicules exhibit multi-component characteristics, indicating concurrent motion in both left and right-handed directions. This simultaneous movement can be interpreted as either twisting or untwisting of the threads[97]. The quantity of turns is related to the overall diameter of the spicule. Figure 11 represents twisting motions. Twisting motions might be interpreted from Figure 11 [97].

In reference [91] they introduced an enhanced operator known as Madmax (OMC), which identifies maxima of convexities calculated in various directions around each pixel. This operator was rewritten in Matlab and demonstrated to be highly effective for pattern recognition purposes. This algorithm is employed to track the presence of slender, hair-like structures within the chromosphere, such as the thin solar jets or spicules observed in

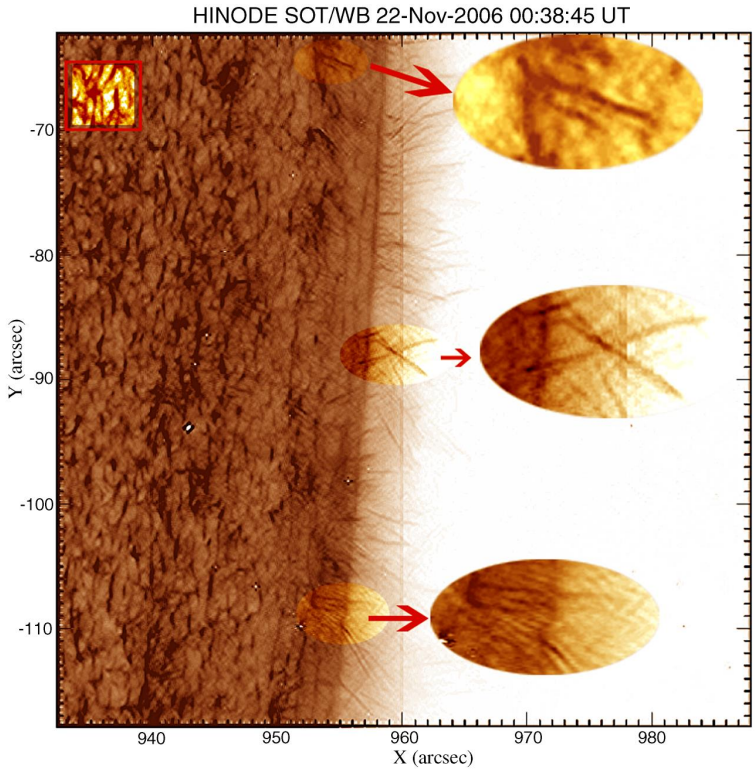

Figure 7: Processed image of SOT/*Hinode* on 22 November 2006 [93].

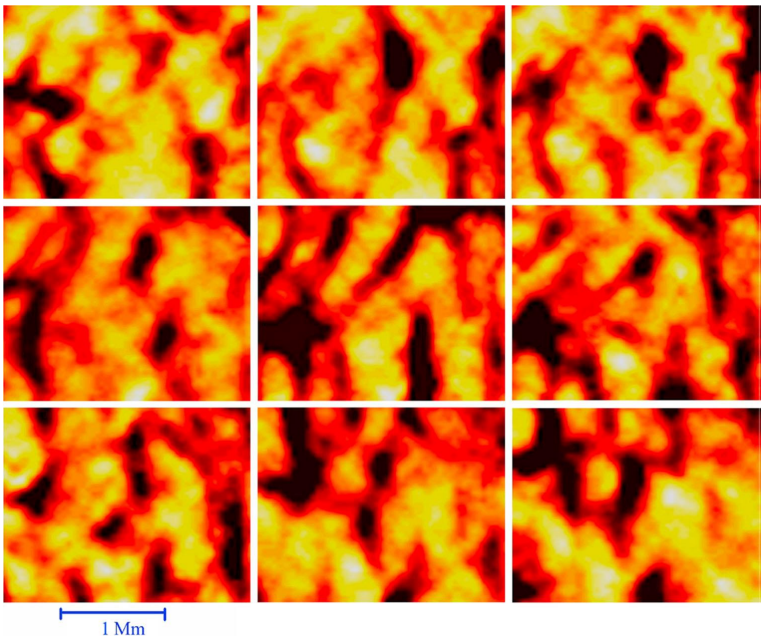

Figure 8: Time evolution of the base of spicules and the splitting processes with a cadence 40 s at 00:24:00 UT. Base of [93].

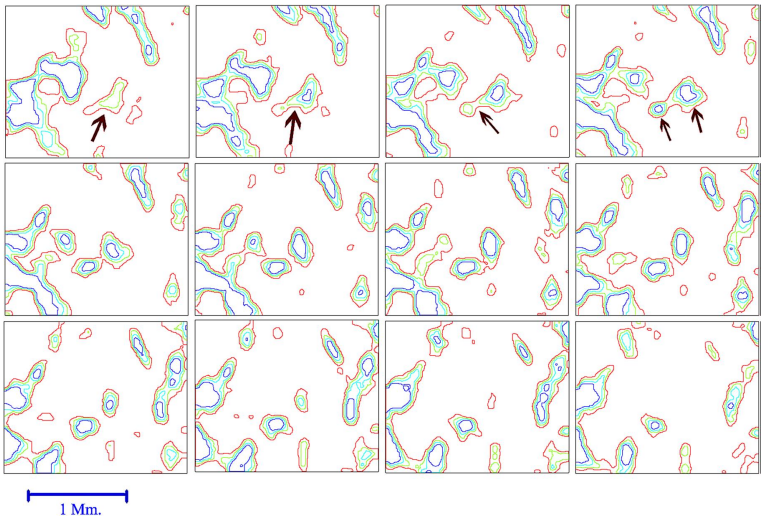

Figure 9: Contours plots of time evolution indicated the splitting one magnetic bright point to doublet points. The cadence of images is 8 s, on 22 November 2006 at 00:45:00 UT [93].

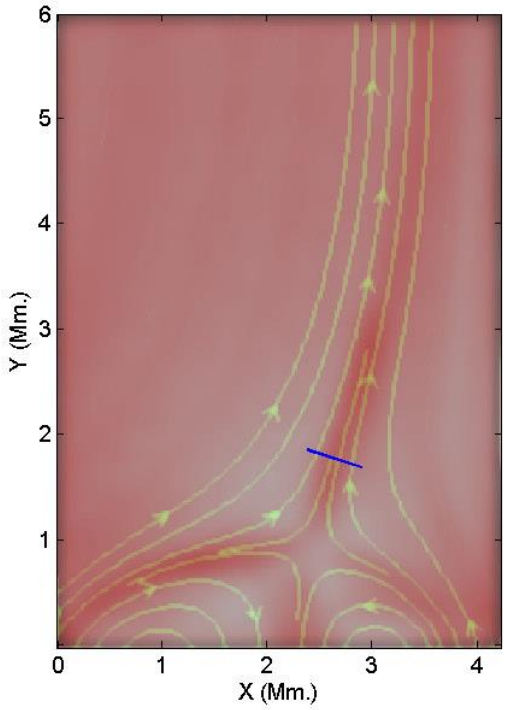

Figure 10: Green stream lines show the magnetic field lines close to the reconnection point. Red lines indicate velocity. The blue line is where the authors study oscillations [92].

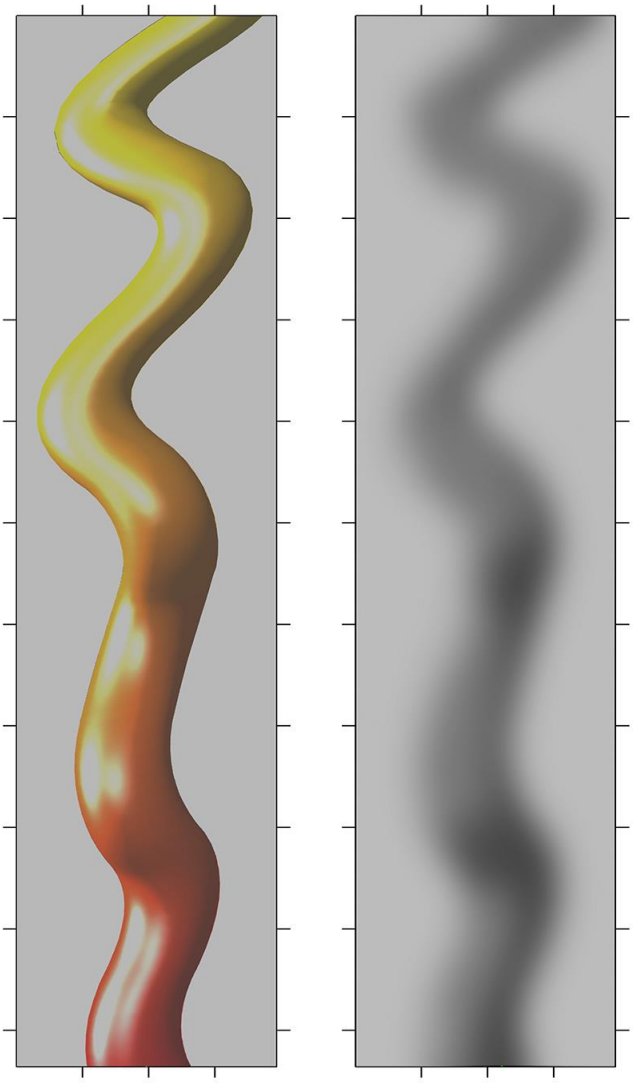

Figure 11: Left: A twisted thread using a propagation of torsional motion. Right: Corresponding 2D negative view supposing the plasma is optically thin at this emission line [97].

high-resolution solar imaging. These observations often suffer from contamination by noise originating from various sources. The key spatial operator utilized in this context relies on the second derivative, specifically chosen in the direction where its absolute value reaches its maximum. Consequently, it leverages the inherent positivity of the resultant intensity signal, even when affected by superimposed noise [3]. In Figure 12, you can observe three sets of images. The first set displays the original test image featuring various textures. The second set showcases the corresponding blurred image, which results from applying blurring effects to the original. Lastly, the third set exhibits the reconstructed image, achieved by utilizing the OMC code (Madmax), but applied to the blurred image. These reconstructions are demonstrated for three distinct tiling steps [91]. In [96] scientists conducted a study to investigate the coherence of intensity oscillations in solar spicules as they extended higher above the solar limb. This research encompassed observations in various solar conditions, including the quiet Sun, the active Sun, and active regions, and utilized data from the Hinode/SOT instrument. In the quest for substantiating the coherence of these oscillations, They employed both Fourier and wavelet analyses to quantify the primary frequency peaks of intensity at various altitudes, along with determining the phase difference between oscillations at two specific heights. The outcomes from their fast Fourier transform (FFT) revealed frequency peaks at approximately 3.6 mHz, 5.5 mHz, and 7.3 mHz across three distinct scenarios. They discovered that the variations in power levels across the three datasets remained unaffected by both altitude and solar activity. Their wavelet analysis yielded dominant frequencies consistent with the FFT results. The coherency results showed frequencies around 3.5 mHz and 5.5 mHz across all three datasets. In a study conducted by [115], the focus was on investigating the contribution of active-region spicules to the mass balance of the solar wind and their role in supplying energy to heat the solar atmosphere. The researchers utilized high-cadence observations obtained on January 26, 2007, from the SOT instrument aboard the *Hinode* satellite, specifically in the Ca II H line filter. This observational technique was chosen due to its ability to provide the necessary high spatiotemporal resolution for the detection of fine structures like spicules. To analyze the data, the researchers employed both Fourier power spectrum and wavelet analysis techniques on the time series data acquired from the active-region observations made by *Hinode*/SOT. Their research uncovered coherent intensity oscillations, which could potentially serve as evidence for the transport of energy responsible for heating the solar atmosphere. To investigate further, they employed time series data and measured the phase difference of these oscillations between two distinct heights, with a focus on how it varied with frequency. The outcomes of their analysis, which included both FFT and wavelet techniques, revealed distinct peaks in the power spectrum within the frequency range of 2 to 8 mHz at four distinct heights above the solar limb. According to their findings, approximately 0.02 to 0.1 of the spicule mass migrates towards the solar corona, while the remainder returns to the chromosphere. In simpler terms, spicules have the capacity to replenish the mass lost as a result of the slow solar wind [115].

2 Bright Points Ejections

When solar chromosphere is observed in the quiet Sun (QS), it is seen as dominated magnetic bright points (MBPs) or magnetic network at rosettes of supergranules [36], [92]. Solar magnetic field extent from the photosphere, chromosphere, TR, and corona into the interplanetary space. Beyond active regions and sunspots, the area of the solar surface is referred to as the "quiet Sun" (QS) [70]. The network exists beyond the confines of the supergranules. Throughout the lifespan of the network, it undergoes dynamic spatial and

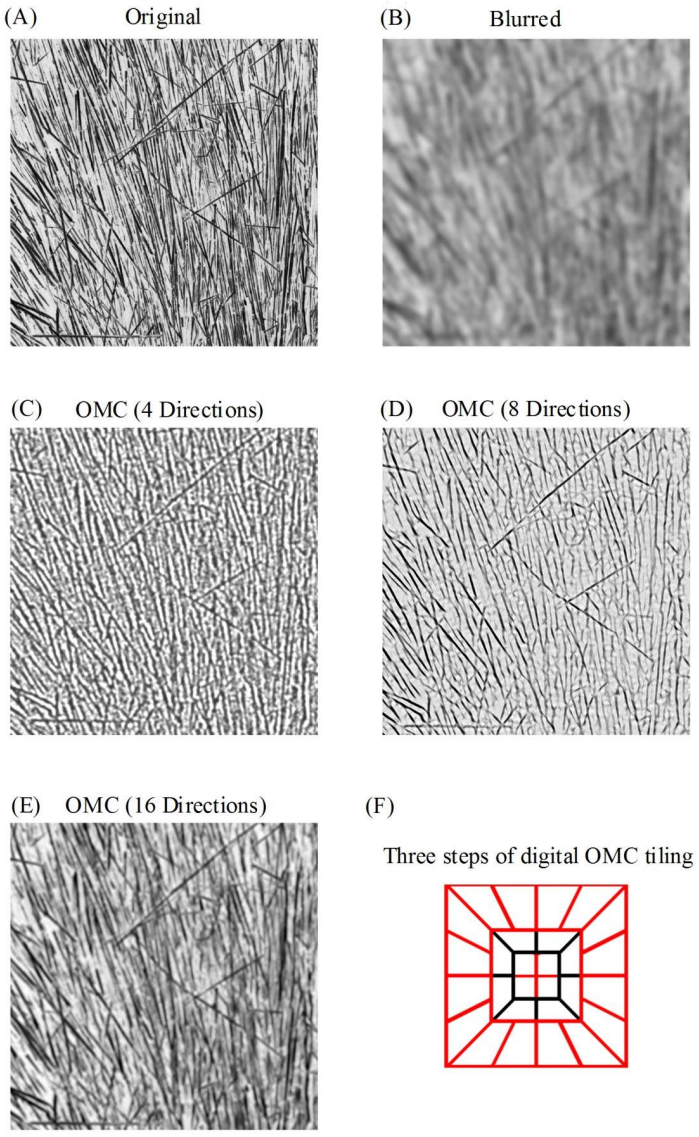

Figure 12: Step by step applying the OMC code (Madmax) to the original image [91].

temporal alterations [76]. Internetwork is the region inside the supergranules. Within the internetwork, there exist discrete magnetic fields. Due to the motions of the magnetic field an effective flux transportation observe at the network [60]. There are magnetic field in the both internetwork and the network [35], [49], [50]. In a study by [10] the lifetime of Bright Points (BPs) was documented as being less than 120 seconds, as observed through the New Solar Telescope (NST). [113] identified a lifetime of approximately 131 seconds for chromospheric Bright Points (BPs) observed by Hinode/SOT. Magnetic field is strong in Bright points (BPs) and ARs, explosive events (EEs), CHs, and the QS network and internetwork brightness. Bright points sizes mostly change with spatial resolution of the imaging instrument. [10] determined the size of BPs as 77 km by the New Solar Telescope (NST). According to [107], the mean diameters of Magnetic Bright Points (MBPs) were reported to be approximately 166 kilometers, as determined from observations made with the Hinode/SOT instrument. [107]and [113] measured diameter of MBPs under 70 km and 210 km respectively. Confined flux tubes play a crucial role in transporting large-scale and long-term magnetic fields throughout the solar atmosphere. This is because Magnetic Bright Points (MBPs) exert control over the diffusion mechanisms, and the flow of Bright Points (BPs) serves to concentrate magnetic flux into a network-like pattern. So far, many simulations of solar MBPs made to indicate the dispersal, concentration, and diffusion of magnetic flux. Researchers in [18] examined the impact of these changing trajectories on an initially uniform and randomly distributed collection of tracer points. The visualization revealed how Bright Points (BPs) evolved within all the datasets, transitioning from a random and uniform distribution to a discernible network-like structure. This concentration of points occurred at the vertices of the flow pattern. It's worth noting that these points are not accurate representations of Bright Points associated with strong magnetic fields. For relatively weak fields these models were very accurate. MBPs were firstly described as magnetic elements. Usually, network MBPs observe more intense and dense than the internetwork areas [5], [81]. In [100], it was found a robust correlation between bright points and high Doppler velocities. This finding serves as compelling evidence of their association with strong magnetic sources. A dominant period of oscillations about 3 min have seen in the chromosphere, which is often seen in velocity and intensity in Mg II h and k spectral data [84]. The 5-minute oscillations primarily originate in the photosphere and the lower chromosphere. These oscillations are commonly referred to as p-modes [61].

Photosphere BPs and chromosphere MBPs may not definitely related together [64]. By using spectroheliograms, it is confirms a strong relation between chromosphere network magnetic BPs and the QS supergranulation process, dopplergrams, and magnetograms. However, the theoretical understanding of the interaction between the magnetic field within the network ($\sim$ 1 kG) and the dynamic flows at the boundaries of these giant cells is currently lacking. [83] found that there was no matching between supergranulation and the magnetic network. [71] suggested that the magnetic network formation is highly related to supergranulation flows. [39] indicated that on a large scale, the distribution of coronal bright points (CBPs) on the solar surface is uniform, but in, ARs it is deviated from. Bipolar features seen in magnetograms are signs of X-ray CBPs. The gap between the bipoles widens as their lifespan progresses. This separating motion velocity is about 2 km s^{-1}. A typical magnetic flux is ranged from 10^{19} to 10^{20} Mx per day of lifetime. In their study, [62] documented the convergence of bipoles and the cancellation of magnetic elements with opposing polarities. Meanwhile, [52] observed that certain Coronal Bright Points (CBPs) are generated through the convergence of bipolar magnetic fields, while others arise from the emergence of entirely new magnetic fields. [55] provided evidence for the soft X-ray brightening events, which are called coronal flashes. The feature had a short lifetime and could be related to X-ray jets. [75] found that a CBP consists of several miniature loops (each $\sim$ 25 Mm in diameter and

12 Mm long). [6] and [9] indicated that there are two main group of a lifetime for CBPs. About 52 percent showed typical short lifetimes of less than 20 minutes and 48 percent showed long lifetimes of 6 hours. For finding sources and physical properties of CBPs, it is necessary to identify and track the bases of the CBPs. In their study, [8] employed an automated approach that relied on Zernike moments and a Support Vector Machine (SVM) classifier for the purpose of detecting and tracking solar campfires as observed by the Solar Orbiter's Extreme Ultraviolet Imager (EUI) and the Solar Dynamics Observatory's Atmospheric Imaging Assembly (AIA). A notable portion of the HMI (Helioseismic and Magnetic Imager) Magnetic Bright Points (MBPs), which are predominantly characterized by small-scale bright dots, exhibit a tendency to reappear in approximately the same areas within the photosphere. These characteristics are linked to Transition Region (TR) Dopplergrams that feature regions with elevated Doppler velocities. [98] suggested that some of these BPs are duo to magnetic reconnections of loops at base regions in the lower layers of TR and chromosphere. Because of inaccessibility in the measurement of the coronal magnetic field, understanding the correct magnetic structure and properties only through the characteristics of the surrounding the magnetic structure is indirectly identified. [38] depicted the geometric characteristics of solar jets, showcasing a prominent upward ejection of hot plasma into the higher layers of the solar atmosphere. This phenomenon has the potential to induce abrupt heating of the solar corona and contribute mass to the solar wind. It is reasonable to anticipate that these Coronal Bright Points (CBPs) could also be traced throughout the Transition Region (TR) and chromosphere, given the continuous expansion of photospheric magnetic field lines toward the corona. It's worth noting that Dopplergrams have been a long-standing and established technique for studying supergranulation. [81] determined that the typical length of this structure ranges between 20 and 30 Mm. In the study described in [100] the authors explored the connection between the photospheric magnetic field and Dopplergrams in both the chromosphere and the Transition Region (TR) for observations made in Near Ultraviolet (NUV) and Far Ultraviolet (FUV) channels. They also examined how these observations correlated with filtergrams taken in the Extreme Ultraviolet (EUV) range to better understand the relationship between different layers of the solar atmosphere. [11] estimated the chromosphere mass velocity of about 20 km s^{-1} using FLCT method. In the field of solar physics, it is imperative to comprehend the mechanisms by which energy is conveyed into the solar corona and how it propagates along magnetic field lines spanning from the deep photosphere, through the chromosphere and the Transition Region (TR), and ultimately into the corona. Understanding this energy transport process is crucial for gaining insights into the dynamics of the Sun's outermost layers. A highly effective method for studying energy transport is through the use of *Interface Region Imaging Spectrograph* (IRIS) raster scans and imaging observations, particularly in the near-ultraviolet (NUV) and far-ultraviolet (FUV) emission channels. These observations offer exceptionally high time and spatial resolutions, making them a valuable tool for investigating the dynamics of energy transfer within the solar atmosphere. Researchers in [100] examined the quiet Sun using data from the *IRIS* specifically focusing on high signal-to-noise ratio observations in the Si IV, C II, and Mg II k lines, which exhibited strong emission intensities. Their analysis revealed a robust correlation among the bright network points in the Transition Region (TR). Their results indicated that The intensity maps and Dopplergrams obtained from the *IRIS* were contrasted with the corresponding data from the Atmospheric Imaging Assembly (AIA) and the Helioseismic and Magnetic Imager (HMI) instruments, both of which are part of the *Solar Dynamical Observatory* (SDO) mission (see Figures 14-16). Additionally, they demonstrated that the mean intensity profiles of the network exhibited a significant correlation with the coronal channels of the Atmospheric Imaging Assembly (AIA). Moreover, they utilized simultaneous observations of the magnetic network from the

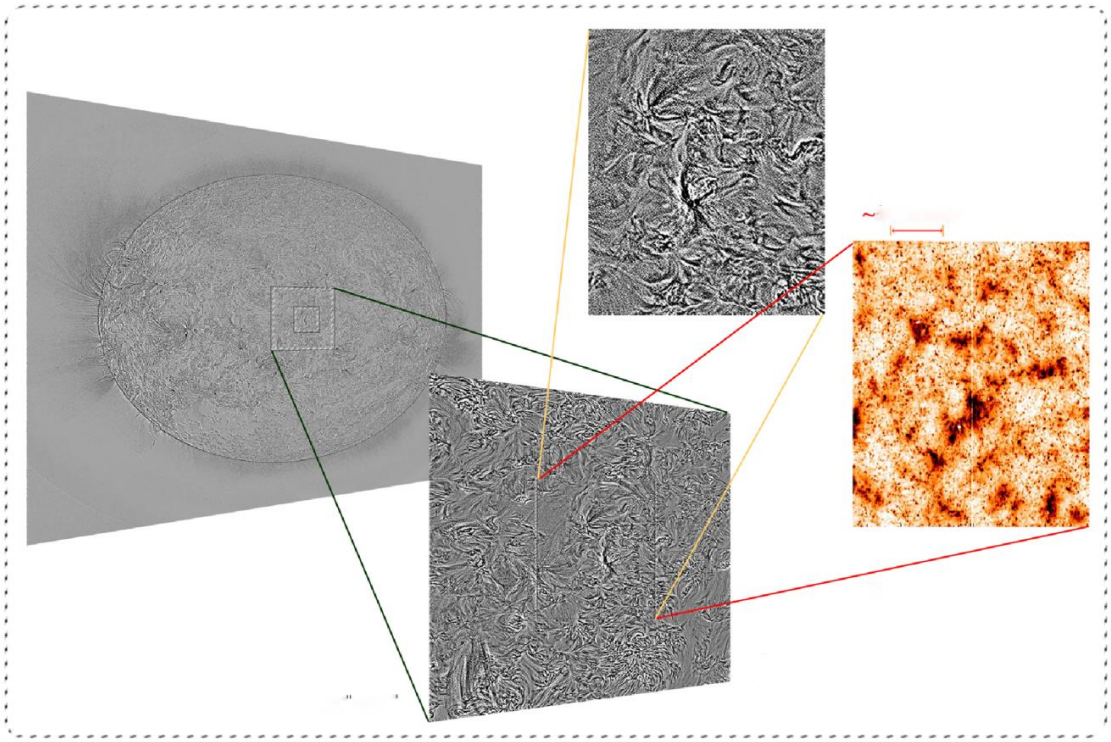

Figure 13: The full disk image of SDO/AIA filtered in Fe IX 171 Å. The right panels indicate *IRIS* images in several TR lines [100].

Helioseismic and Magnetic Imager (HMI) and identified a robust connection between the network's Bright Points (BPs) across various layers of the solar atmosphere. These network elements displayed prominent characteristics, including regions of high Doppler velocities and substantial magnetic signatures.

In order to investigate the movements and oscillations occurring within the solar chromosphere and Transition Region (TR), researchers in [101] conducted an analysis of significant off-limb Doppler shifts observed using the *IRIS*. They used raster scans and SJI observations performed in the near-ultraviolet (NUV) channels. They found large transverse oscillations in far wings profiles. In the tranquil regions of the Sun, particularly in the polar Coronal Holes (CHs), researchers conducted an analysis of the dynamic characteristics of the dispersed material associated with spicules, using high-resolution *IRIS* observations that offered precise spectral, temporal, and spatial data. Their findings pointed to the presence of numerous small-scale spicules exhibiting swift twisting and swaying movements, as evidenced by the notable distortion and dispersion of their spectral line profiles, along with remarkable periodic Doppler shifts. They also noted that the majority of these spicules appeared repeatedly, displaying both red- and blue-shifts above the solar limb during the entire observation period. The average swaying speed of order ± 35 km s^{-1} reached a maximum value of 50 km s^{-1} in the polar CHs, well above the 2.2 Mm heights were obtained. Additionally, they made a groundbreaking discovery by identifying waves with exceptionally short periods, measuring just 100 seconds or less. They computed transverse amplitudes in the range of $\pm$ 20 to 30 km s^{-1} displaying clear characteristics indicative of Alfven waves.

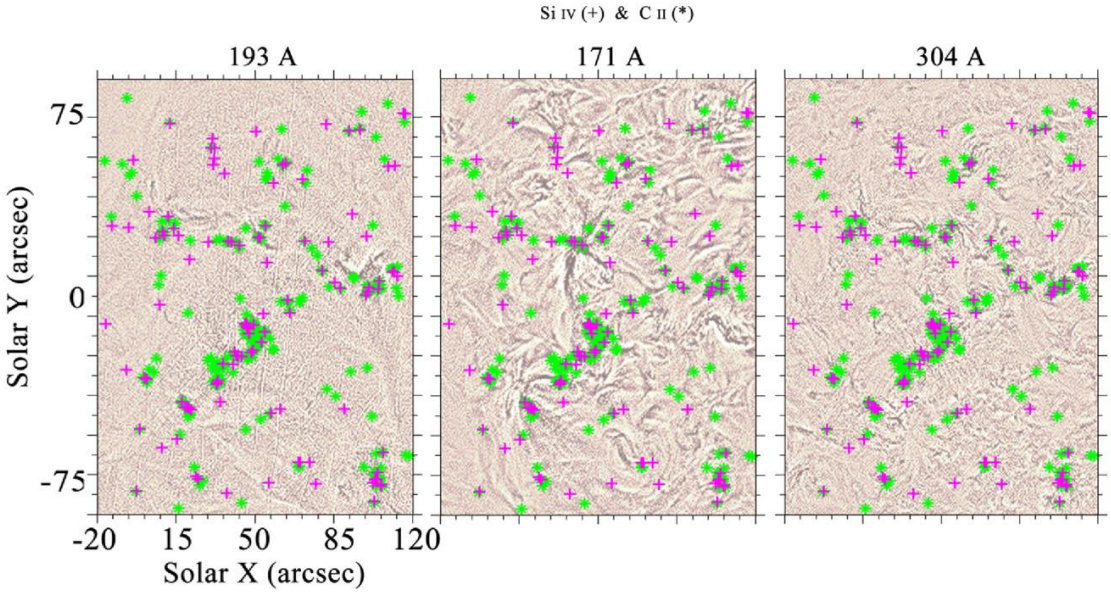

Figure 14: The *IRIS* images of BPs in TR, and AIA/SDO images show a significant 2D correlation. Results of summing frames for 30 minutes were observed. [100].

See Figures 17-19.

The Sudden rise of solar atmospheric temperature is still unresolved. Waves and instabilities within the solar plasma have been put forward as potential candidates to address this matter. There is a hypothesis proposing that the energy carried by these waves could contribute to heating the solar atmosphere, including the Transition Region (TR) and the corona. Using the *IRIS* telescope observations, researchers in [116] conducted an examination of the waves within magnetic tubes, including UV bright points located at the boundaries and within the supergranules. Investigating these dynamic structures, which exist in the region between the chromosphere and the transition region, holds the potential to significantly enhance our understanding of the transport of mass and energy through the interface region that separates the chromosphere from the inner corona. The magnetic BPs represent the surface manifestations of magnetic flux tubes connected to magnetic features. These flux tubes ascend towards the upper layers of the Sun's atmosphere, presenting themselves as luminous granules that form the chromospheric network. To explore the periodic characteristics of these phenomena and delve into different facets of their oscillations, researchers conducted a detailed investigation. In a study referenced as [116] , they individually analyzed intensity fluctuations using the wavelet analysis technique in the 2796 Å , 1400 Å and 1330 Å spectral lines observed by the Interface Region Imaging Spectrograph (IRIS) Solar-Joint Imager (SJI). They extracted the periods of intensity fluctuations in these points, which ranged from 2 to 8 minutes, closely aligning with the frequencies associated with atmospheric pressure modes. To delve deeper into wave propagation within these atmospheric layers, they explored the correlation of oscillations between the chromosphere (2796 Å) and the transition region TR (1400 Å and 1330 Å) heights using the cross wavelet method. Their findings revealed a strong correlation with periods ranging from 2.5 to 5.5 minutes and wave speeds spanning 30 to 200 km s^{-1}. Additionally, they employed the Si IV line to ascertain the Doppler velocities of the magnetic bright points (BPs) within

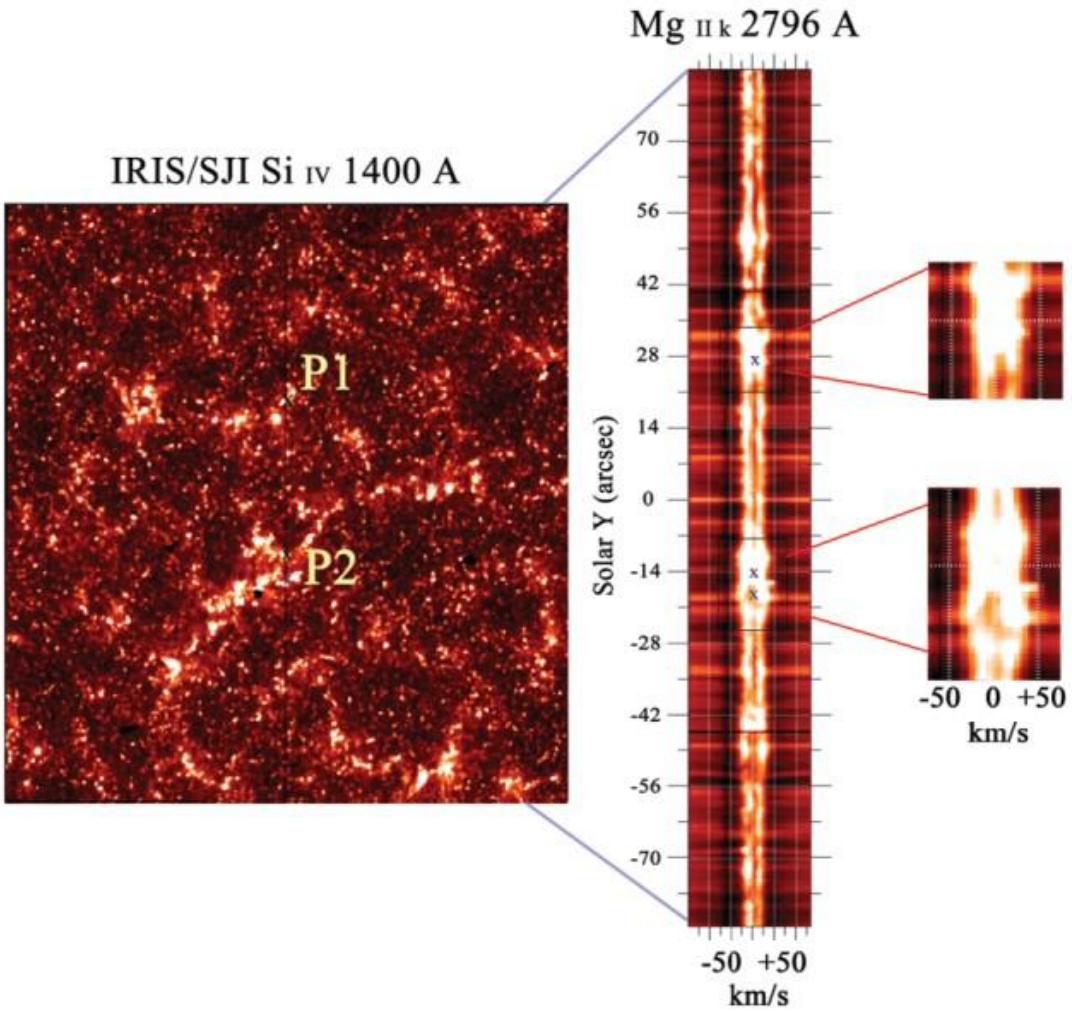

Figure 15: Left: SJI of BPs. Right: Short-lived of BPs is seen as bright features in the blue and red wings (around ± 50 km s^{-1}) in Mg II k 2796 Å spectral line [100].

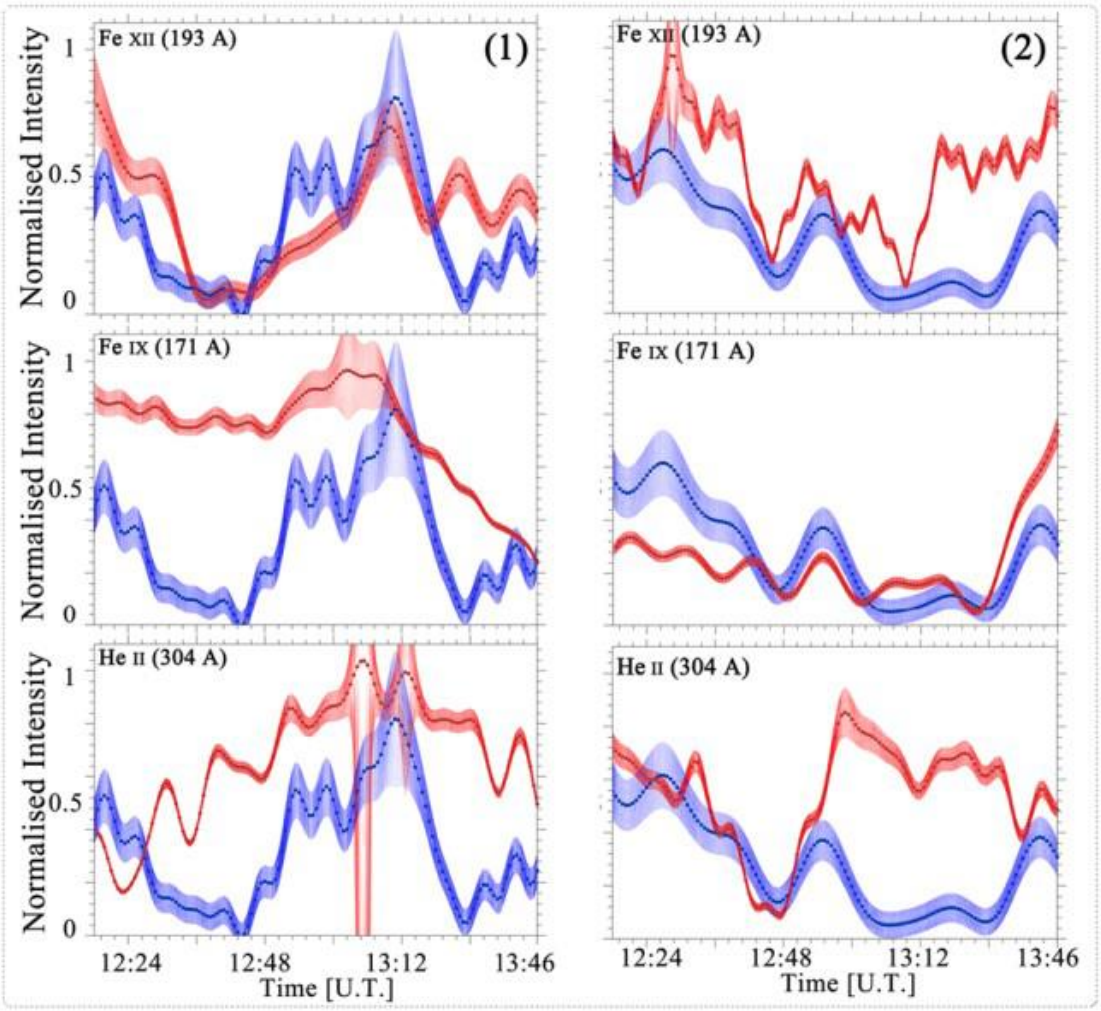

Figure 16: intensity variations in the region which is marked as numbers 1 (left column) and 2 (right column) in Figure 15. The common diagram in all panels (blue squares and confidence bounds) is for *IRIS* Si IV (1400 Å), and simultaneous intensity for AIA channels is illustrated in red [100].

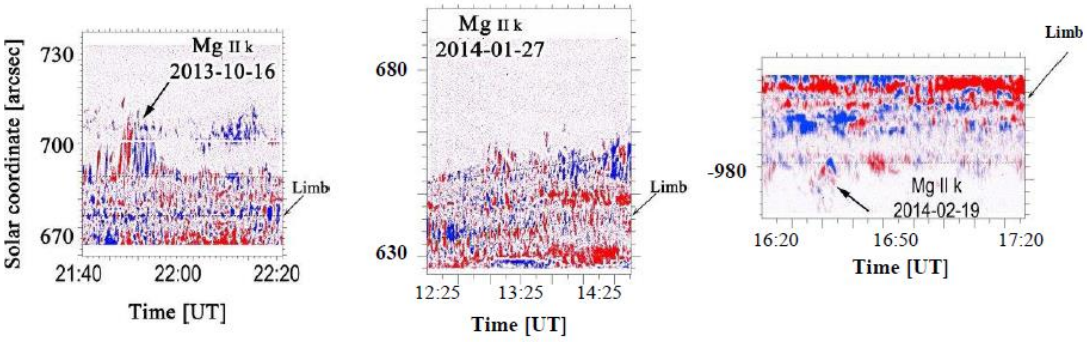

Figure 17: Doppler images obtained by in the wings of Mg II k line (2796.32 Å). The color scale is corresponded to [-30 +30] km s^{-1} or ± 0.3 Å. Solar limb are illustrated by arrow [101].

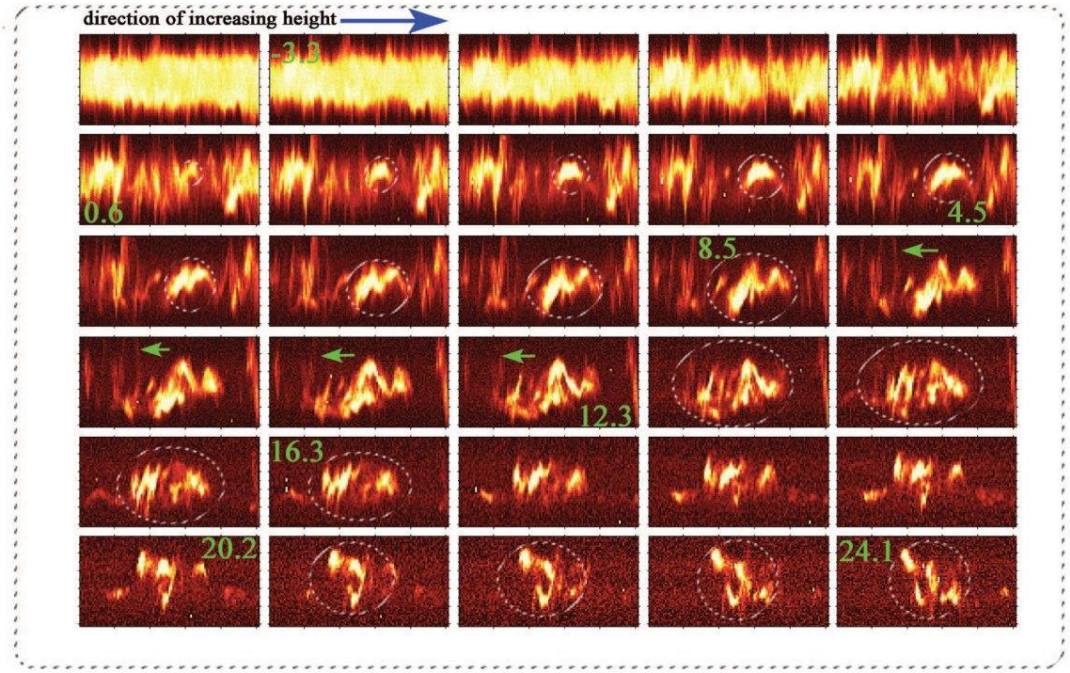

Figure 18: Time evolutions of Mg II k spectra from 16:35 to 16:50 UT on 19 February 2014. The time cadence between panels is ∼ 15 minutes. Height distance between successive panels is 3 pixels or 1 arcsec (pixel size is ∼ 0.33 arcsec). There are the waves with very short periods (< 1 min) between 14 and 18 arcsec [101].

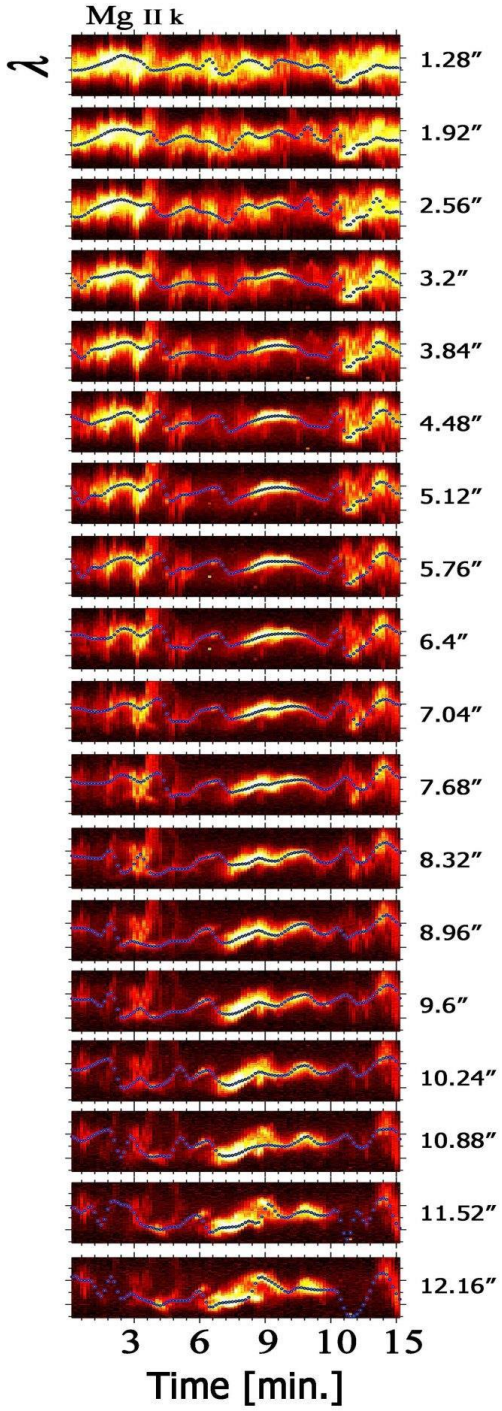

Figure 19: Time evolutions of spectra in Mg II k with a possible reversal of Doppler velocities with heights on 19 Feb 2014 and time interval is the same as Figure 18 [101].

the chromospheric network and internetwork. These velocities were found to range from approximately -20 to 30 km s^{-1} for BPs within the network and from 21 to 21 km s^{-1}, for those in the internetwork. (see Figures 20-22). Their findings imply that the transmission of waves through the magnetic flux tubes carrying upward-flowing plasma within magnetic bright points (BPs) plays a crucial role in heating the solar atmosphere.

[74] investigated oscillations period of BPs in Mg II k line intensity, brightness temperature, and Doppler velocity. They used data from (*IRIS*) and SDO. They identified MBPs in Si IV 1403 Å and SJIs, with the magnetogram information from the Heliospheric and Magnetic Imager (HMI). See the Figures 23-24. For detecting the oscillations they work on Y-T analysis by wavelet method on the Mg II k 2796 Å and 10,000 K. A power spectrum analysis was conducted to delineate the oscillatory behavior of various regions. The results revealed distinct characteristics: network points exhibited a recurring intensity, temperature, and velocity oscillation with an average period of approximately 300 seconds, while internetwork points displayed an average intensity oscillation period of roughly 180 seconds, a mean temperature oscillation period of about 202 seconds, and an average velocity oscillation period of approximately 202 seconds.

It is believed that many bright features in the chromosphere play a basic role in the heating corona. Examining the wave properties within the outer layers of the solar atmosphere is instrumental in gaining a deeper understanding of this region. Among these properties, the wave phase speed (PS) stands out as a pivotal factor influencing both solar coronal heating and the distribution of energy throughout the solar atmosphere. [73] determined energy flux (EF) of BPs calculating the filling factor and the phase speed. They obtained filling factor by the size and intensity of the *IRIS* BPs. They calculated Doppler velocity from 40 to 180 km s^{-1} at the network and from 30 to 140 km s^{-1} at the internetwork. In the AR, they obtained from 80 to 540 km s^{-1} at the network and 70 to 220 km s^{-1} at the internetwork. They obtained the EF for the *IRIS* BPs in three different frequencies. Their results confirm that energy flux of the network BPs can heat solar atmosphere temperature.

Researchers in [119] studied a set of bright spots that were recorded on 17 August, 2014 at 2796 Å, 1336 Å, and 1394 Å wavelengths. They employed the temporal evolution analysis method to monitor the trajectory of these structures and ascertain their apparent velocity. Simultaneously, they determined the Doppler velocity by utilizing Gaussian fitting of spectral intensity profiles. Their results of apparent speed showed that these jets have speeds of approximately 10 to 110 km s^{-1} . Analysis of the spectrum of the blue and red wings (line of sight velocities) at three wavelengths showed that these bright spots are moving at Doppler velocities of -65 to 40 km s^{-1}, -60 to 50 km s^{-1}, and -80 to 60 km s^{-1}, respectively(see Figures 25-27). The findings of this study demonstrated that by leveraging data from the IRIS Telescope, it becomes feasible to discern and isolate the distinct physical components of jets across various wavelengths, while also elucidating their dynamic characteristics. These specifications serve as valuable tools for enhancing our comprehension of the layered structure within the solar atmosphere, shedding light on the mechanisms governing the transfer of heat and matter to the solar surface. Furthermore, they enable us to investigate the repercussions of these transitions and their impacts on the Earth's atmosphere. The practical implications of this research extend to the objectives of space exploration and hold significant relevance in understanding the climates of space, Earth, and other planets.

3 Explosive Events

[20] defined Explosive events (EEs) as structures indicating high turbulence in small areas having broad profile and jets with upward-moving material with velocities exceeding

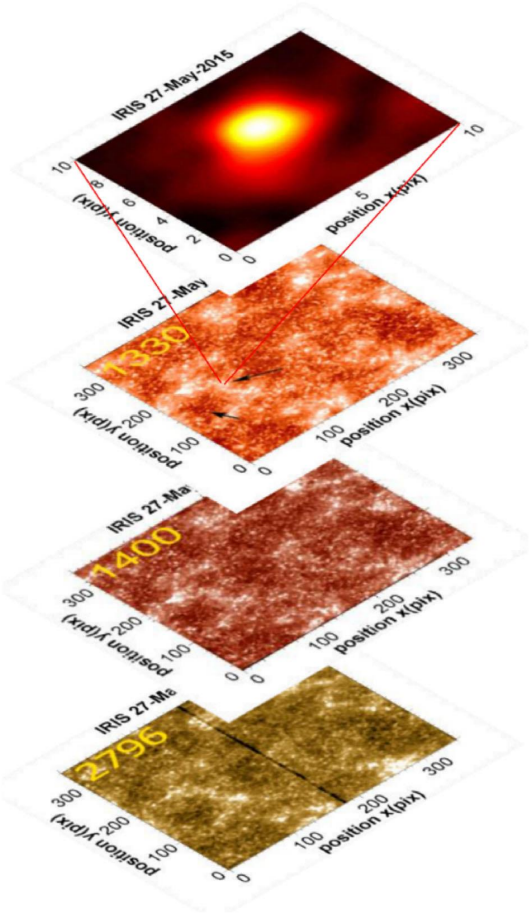

Figure 20: A sequence of images captured on 27 May, 2015 at 11:56 UT by *IRIS*/SJI instrument, showcasing various wavelengths, including 2796 Å(bottom image) , 1400 Å and 1330 Å as we ascend from the solar surface to higher altitudes , and an illustrative instance of a magnified Bright Point (BP) situated along the network boundary. In the lower panel, the locations of two Bright Points (BPs) is observed: one situated along the network boundary, and another within the internetwork, indicated by the two black arrows. Both horizontal and vertical coordinates are provided in pixels [116].

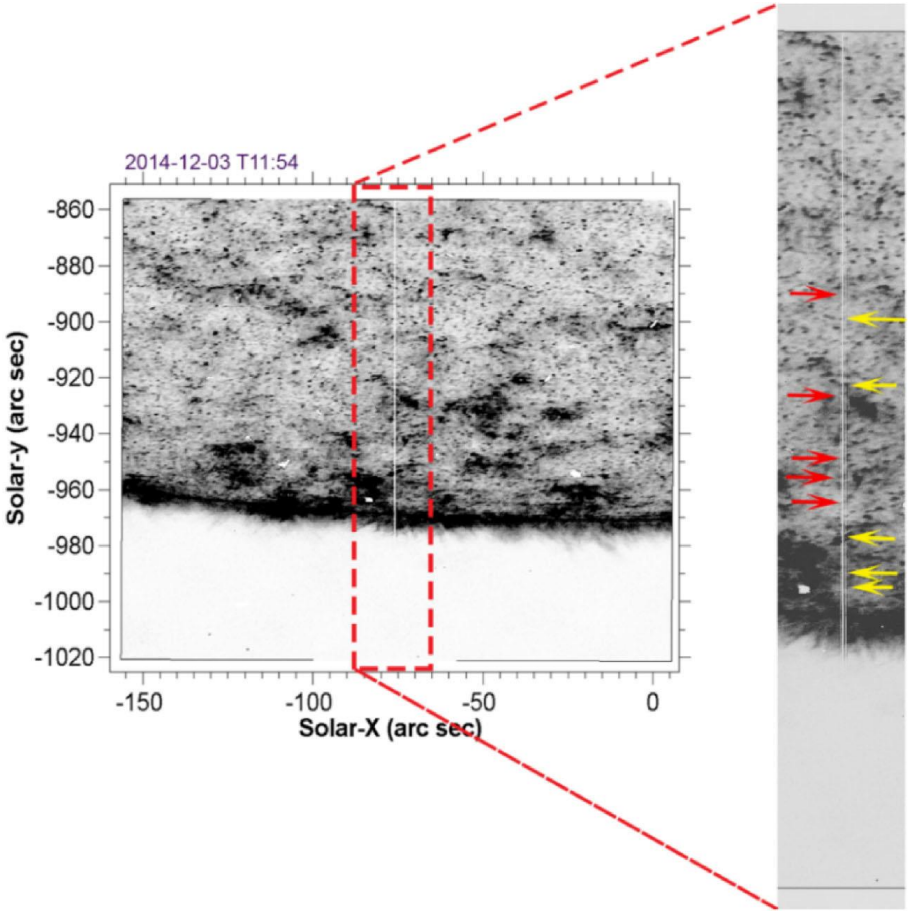

Figure 21: Negative image acquired by the *IRIS* instrument in the 1400 Å (Si IV) wavelength range on 3 December 2014. On the right-hand side, an enlarged view of the area within the red box is seen. The red arrows indicate the locations of Bright Points (BPs) within the network and the yellow ones show (BPs) internetwork regions. Additionally, the vertical white line running perpendicular to the limb represents the position of the slit. [116].

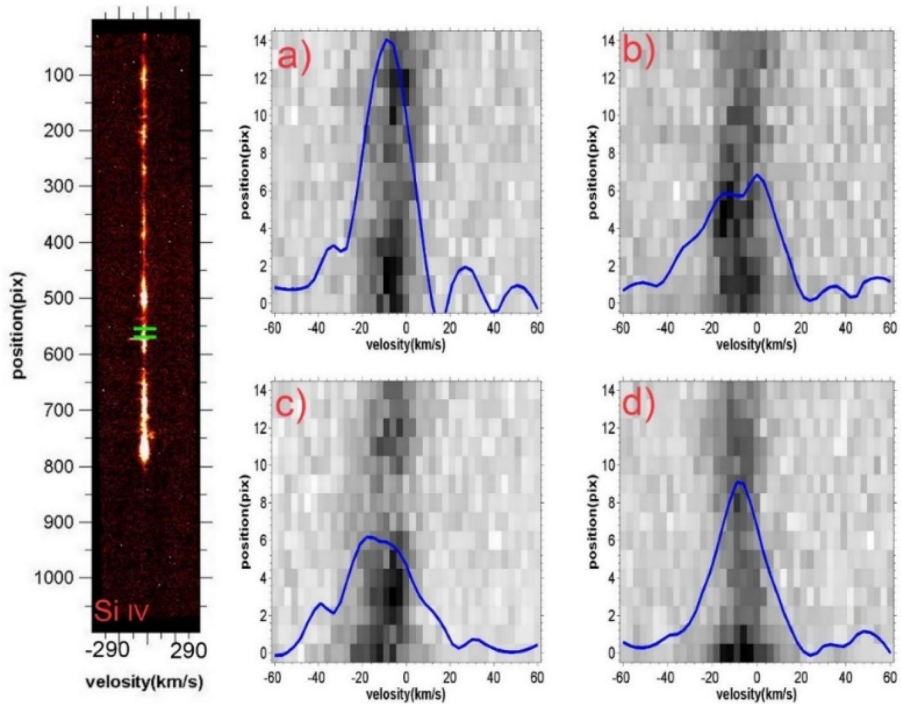

Figure 22: An instance of the *IRIS* spectra obtained from the Bright Point (BP) located within the network, specifically within the spectral windows of Si IV 1400 Å recorded on December 3, 2014. In the panel, two brief green lines is observed, indicating the designated region under analysis. Panels (a)-(d) display the profiles captured by the IRIS spectrum at the slit position, which is demarcated by the two brief green lines illustrated in the left-hand panels [116].

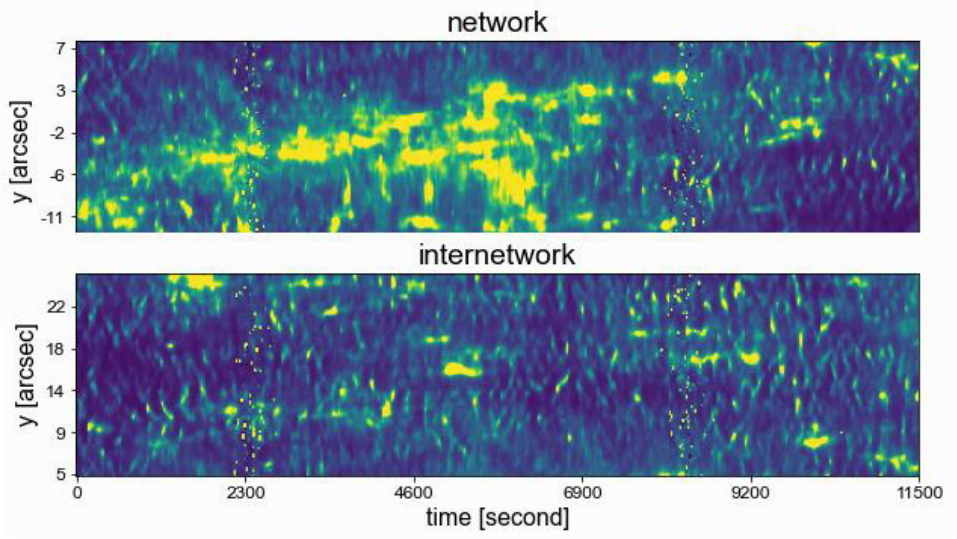

Figure 23: Top panel indicate y-t panel MBPs at network obtained from SJIs 1403 Å; Bottom panel: shows MBPs at internetwork clipped to the range between 0 and 117 [74].

the sound velocity ($\sim$ 120 km s^{-1}) in the corona. EEs were characterized using on-disk far-ultraviolet observations conducted in emission lines originating from the hot transition region. These emission lines covered a broad range of formation temperatures, spanning from logT=4.3 to 5.7 [19]. Authors in [19] identified EEs on solar disk in a sequence of C IV spectroheliograms. Their results confirmed that above the transition region, there are spikes and jets similar to spicules and macrospicules. This was first discovered in data from the Skylab mission [34]. It was postulated that EEs originated from the eruption of compact loops, each with dimensions not exceeding 3000 kilometers. In [22] the researcher established a spectrum of values encompassing size, shapes, and various other physical characteristics associated with these features. [63] provided observational proof of a connection between macrospicules and X-ray bright point flares. Macrospicules are associated with rapid eruptive events characterized by ascent times of only a few minutes or less. A unique rocket observation, [28] showed that the bulk of spicules is recorded only in background absorption outside the coronal organ. Evidence of a connection between hot "jet lets" and soft X-ray transient (SXR) flares was observed from partial frame sequences of the Yokohama mission in the polar regions [55].

From observations of the eclipse, [53] found very thin coronal spikes ($\sim$ 1 arcsec) of white light rising to coronal temperatures above the polar chromosphere. The reason these spikes were visible was because of Thomson scattering occurring at altitudes ranging from 5 to 20 million meters above the solar surface. Their densities are on par with those of the jets, measuring at approximately ($1\times$ 10^{10} cm^{-3}). Moreover, the height of these spikes closely resembles that of the largest jets previously documented by [20], as observed in C IV (logT=5) spectroheliograms [19]. Ground-based telescopes detected off-limb macrospicules and surges in polar regions using hydrogen-alpha (Ha) and other low-excitation spectral lines. In the study referenced as [40] a comparison was made between He II 304 Ångström images obtained from the Extreme Ultraviolet Imaging Telescope (EIT) aboard the Solar and Heliospheric Observatory (SoHO) and those acquired using the Dunn Solar Telescope

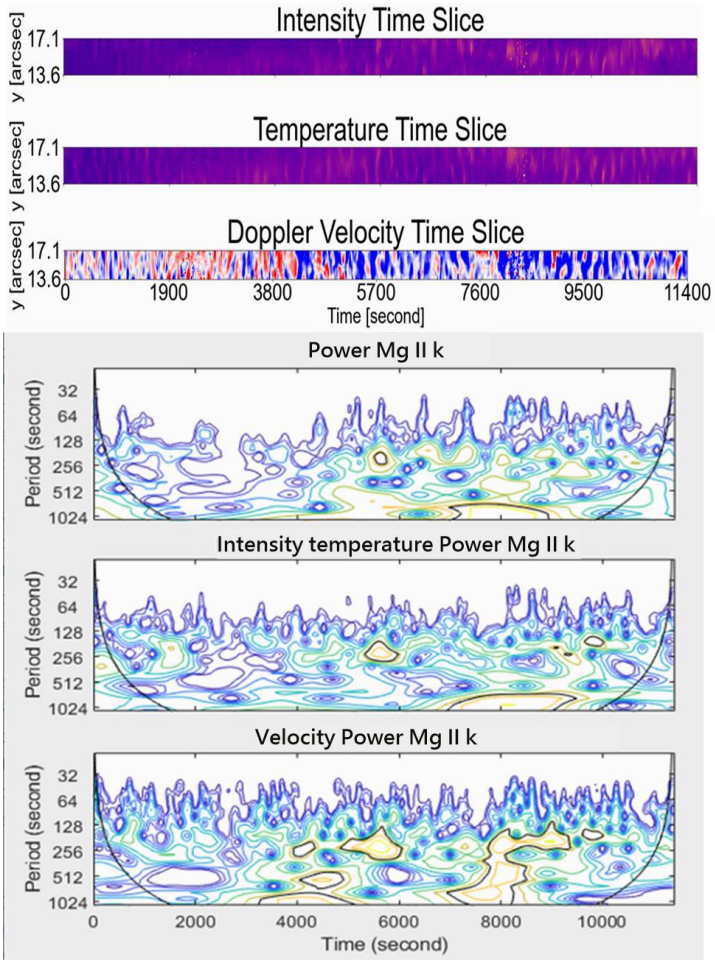

Figure 24: From top to bottom show brightness intensity time-slice, brightness temperature time-slice, Doppler velocity time-slice obtained from a line of sight (LOS) line shift velocities clipped into a range of $\pm$ 13 km s^{-1}, intensity power diagram, intensity temperature power diagram, velocity power diagram for Mg II k spectra respectively [74], [103].

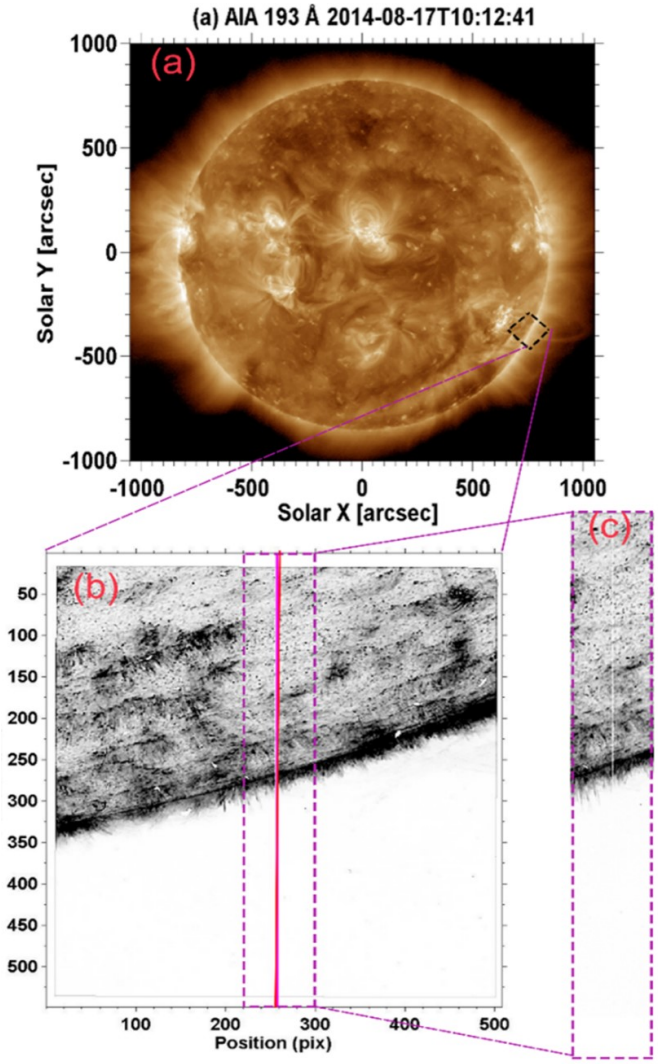

Figure 25: (a) The solar disk image (at 193 Å) taken from the SDO/AIA on 17 August, 2014 at 10:06:13 UT, black square of the study area. (b) shows the magnified image of the black square of Rank and the purple vertical line shows the position of the telescope slit. (c) refers to the active area near the gap [119].

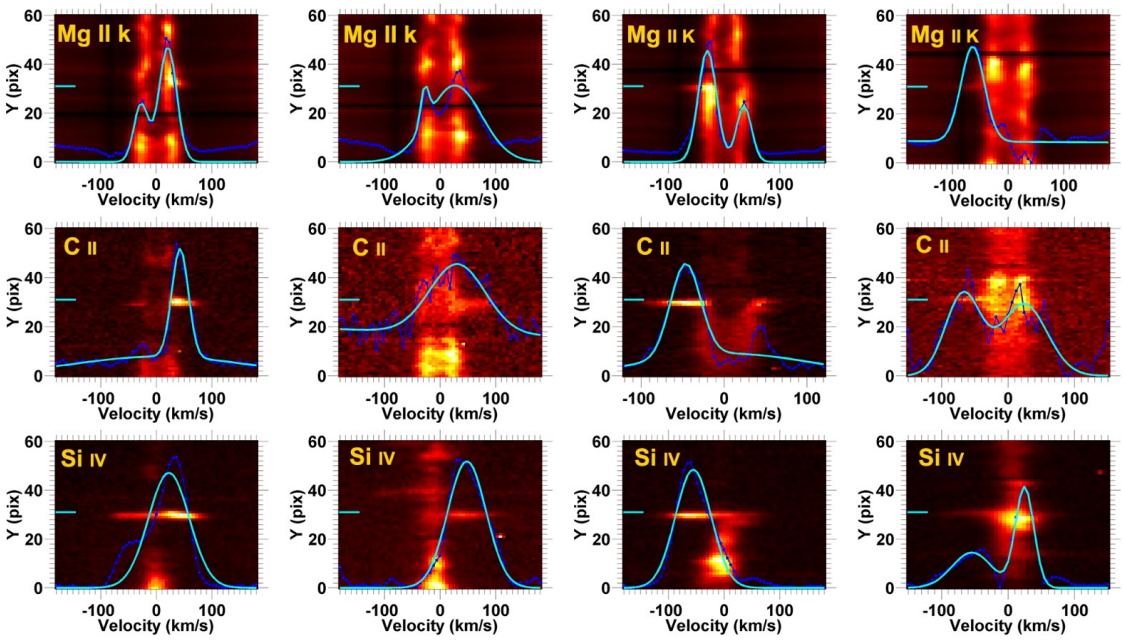

Figure 26: Linear profiles of Mg II k, C II and Si IV related to the first 4 bright spots. From top to bottom, the spectral images of Mg II k with a wavelength of 2796 Å, C II with a wavelength of 1336 Å and Si IV with a wavelength of 1393 Å, on which the spectral intensity profiles along the short cyan line (on the left side of the figure) is drawn [119].

in conjunction with the Universal Birefringent Filter (DST-UBF) at the National Solar Observatory (NSO) located at Sacramento Peak. The images included complex eruptions in the polar regions with large amplitude motions. In polar coronal holes, there are conspicuous small radial jets that may have connections to Hα polar limb surges,as suggested in [54], [40]. These jets are especially noticeable in areas where the Yohkoh mission captured transient soft X-ray (SXR) brightenings, as documented in images from reference [55]. Additionally, these jets are closely associated with the nearby presence of minute bright loops, as observed in calcium II H images obtained by the Solar Optical Telescope (SOT) of the Hinode mission in polar regions, as described in references [88], [98]. The suggestion is that the geometric configuration of these jets, along with their positions, originates in close proximity to singular null points within the coronal magnetic field. [27] discovered a substantial quantity of events occurring either in close proximity to or beyond solar plages on the solar disk. These events featured notable velocities in the apparent outflows, suggesting that these jets could potentially play a role in generating the high-speed solar wind.

There has been a proposal that magnetic reconnection could serve as a plausible mechanism for the generation of spicules or solar jets, as [108], [43], [119], [118]. Classical spicules have been observed in cooler, low-excitation spectral lines such asHα and Hβ of H I , as well as in He I lines. These include high first ionization potential (FIP) lines, which have energies exceeding 10 electron volts (eV), and low FIP lines, including the prominent resonance lines of calcium II (Ca II) in both the ultraviolet (UV) and the infrared (IR) portions of the spectrum. The reviews on spicule morphology, encompassing their derived physical characteristics and dynamic behavior, are detailed in references [85] and [106] . It is well-documented that solar jets exhibit bidirectional plasma flows when they reach their

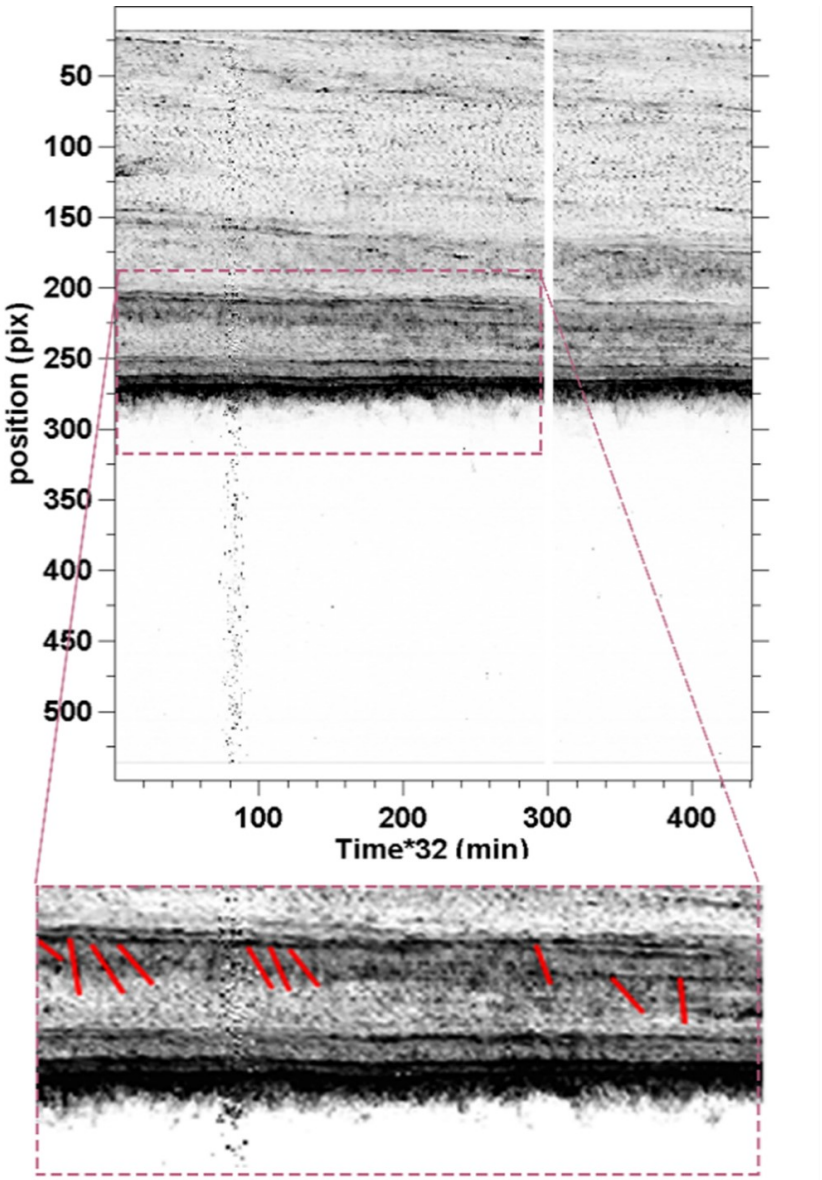

Figure 27: Above shows the image of the time slice along the telescope slit. The horizontal axis is time and the vertical axis is position in pixels. The dotted rectangle shows the time section of the bright spots of the active area under study. The bottom figure is a close-up of the upper rectangle. The red tracks show the traces of bright spots [119].

maximum altitudes [66]. [48] This observation aligns with the magnetic reconnection scenario initially proposed by [48]. [106] documented a comparable phenomenon occurring in on-disk mottles. It has been observed that chromospheric bright points (BPs) tend to appear in locations where arch-shaped mottles are emerging, implying that the presence of these BPs is a consequence of magnetic reconnection, as discussed in reference [82]. [37] found that the current sheet provides high acceleration of charged particles as the case for larger scale events. Erupted small loops in the chromosphere appear to be important in many X null-point reconnection sites [79]. Both [27] and [38] documented the presence of plasma jets spanning a wide range of sizes in their X-Ray Telescope (XRT) observations aboard the Hinode mission. These jets included large X-ray jets as well as numerous smaller ones resembling the typical dimensions of macrospicules. In contemporary observations, macrospicules are consistently detected through full-disk imaging experiments, such as those conducted during the SDO/AIA mission, utilizing the emission line at 304 Ångströms corresponding to He II resonance.

Due to the higher resolution of structures outside the off-limb, it is possible to better describe all bright events, which are related to the height parameter, in the case of observations with high enough resolution to resolve the involved reconnection regions. The analysis focused on events captured in a series of closely spaced rasters taken near the central meridian and the limb near the South Pole. In their investigation, they utilized data from the Solar-Joint Imagers (SJIs) and simultaneously conducted rapid spectral observations. Their findings revealed the presence of Doppler shifts, notably consisting of a pair of red-shifted elements and a faster blue-shifted element originating from nearly the same spatial location. These shifts corresponded to projected velocities of up to 100 km s^{-1} on the plane of the sky. Their results showed bidirectional plasma jets ejected from a small reconnection site. They explained this phenomenon as a result of corona loop interactions leading to reconnection at adjacent sites.

[102] investigated EEs in the off-limb solar atmosphere, with simultaneous observations of the Si IV, Mg II k, and SJIs of the (*IRIS*), on 17 August 2014, and 19 February 2014, See Figures 28 and 29. The data collected by the *IRIS* can be analyzed to study various aspects of the solar atmosphere, including the movement of solar matter, fluctuations, energy absorption, and the transfer of heat. The underlying mechanisms driving the formation of large-scale solar phenomena, such as flares and coronal mass ejections, may have their roots in these smaller-scale, high-energy events. Consequently, delving into the study of these events can provide valuable insights into the mechanisms governing the transfer of mass and energy from the chromosphere to the transition region and the corona. They acquired intensity profiles by examining spectra at two distinct altitudes: at the solar limb and at a 5-arcsecond distance from the solar limb. Subsequently, they conducted an analysis of the fluctuations in Eruptive Events (EEs) at these two altitudes along the observational slit. Their observations revealed that certain spectral line profiles exhibited enhancements in both the blue and red wings, signifying the presence of upward and downward flows. Additionally, some profiles exhibited EEs in opposite directions within both wings. The presence of swaying and rotational movements in the solar phenomena indicates the potential existence of kink and torsional waves. To quantify these motions, they estimated the amplitude of the Doppler velocity in two datasets collected at different altitudes, yielding an approximate value of around 50 km s^{-1}. Furthermore, they determined the phase velocity of the oscillations through a cross-correlation technique, which yielded a value of approximately 220 km s^{-1}. These findings suggest that the fluctuations observed in Eruptive Events (EEs) are indicative of both swaying and rotational motions.

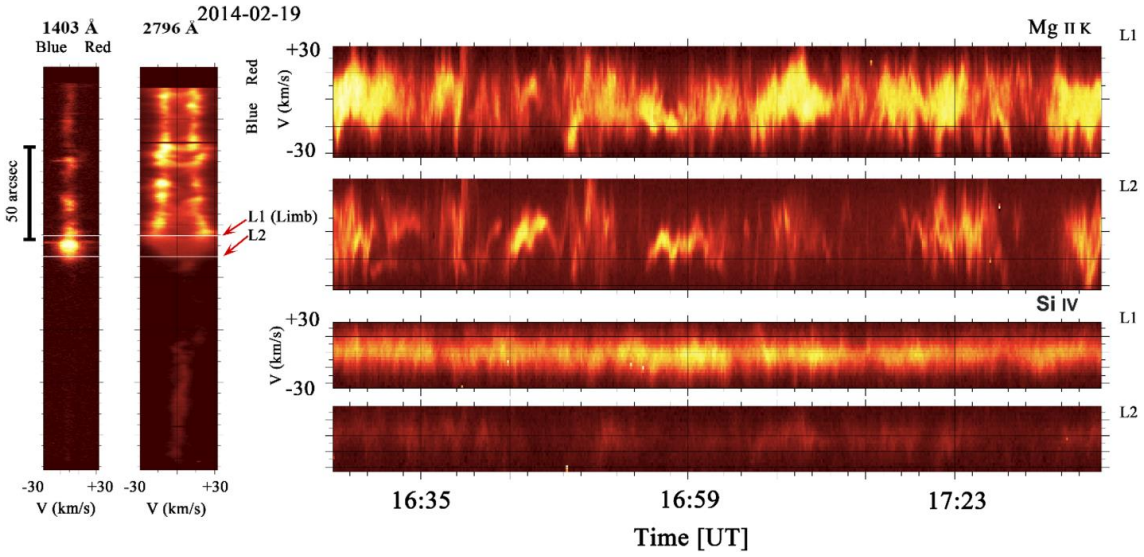

Figure 28: Left panels indicate spectra of Si IV 1403 Å and Mg II k 2796 Å taken on 19 February 2014. The two white lines refer to altitudes along which time slices are calculated. The right panels are the time evolution of Si IV 1403 Å and Mg II k 2796 Å along the two altitudes indicated by two white lines in the left panels. The horizontal lines in the right panels indicate the rest wavelength position Mg II k 2796 Å and Si IV 1403 Å spectra [102].

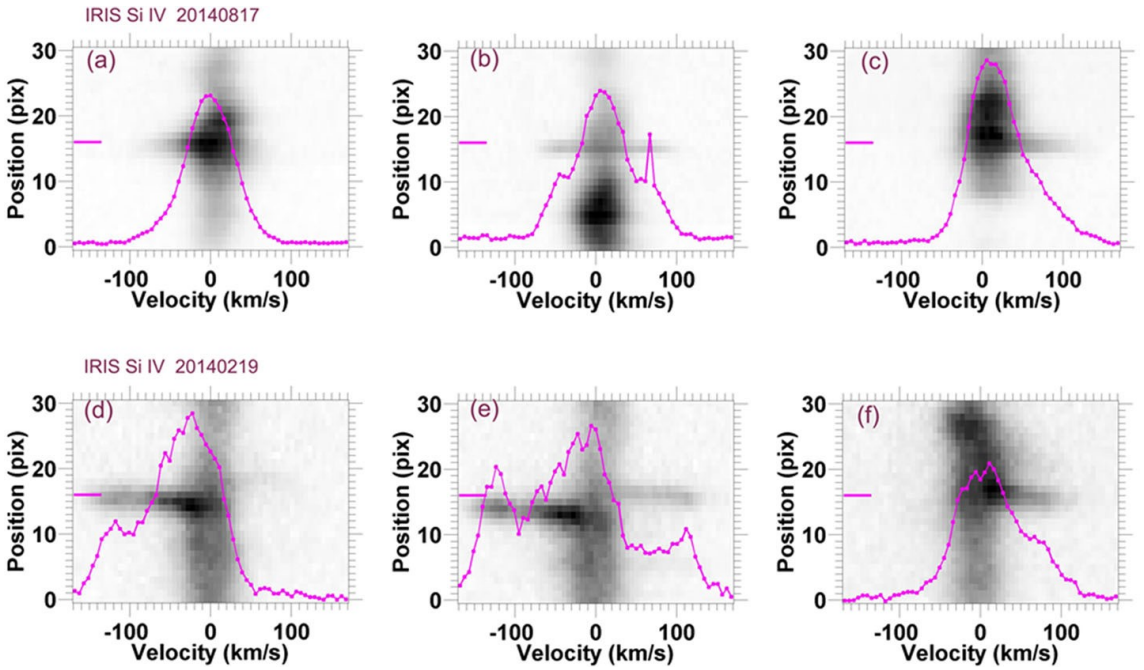

Figure 29: Examples of the EEs with non-Gaussian profiles in Si IV 1403 Å line. Panels (a)-(c) and (d)-(f) obtained from the first and the second datasets respectively [102].

4 Coronal Ejections, CMEs and Solar Activity

Solar flares are the sudden and local brightening of the solar atmosphere, which is evident in the entire electromagnetic spectrum [77]. The energy released by them is more than 10^{25} J within a few minutes through both thermal and non-thermal processes. Coronal mass ejection (CME) is plasma driven from the solar corona into the interplanetary space with a speed of 3500 km s^{-1} and a mass and energy of about 10^{12} kg and 10^{25} J respectively [26] and [111]. Flares are categorized according to their soft X-ray emissions, which are measured in the 1-8Å range and are recorded on a logarithmic scale using data collected by the Geostationary Operational Environmental Satellites (GOES).

Flares are defined as classes X, M, C, B, and A, from strongest to weakest, with decimal subclasses (M1.0, C5.2, etc.). Since flares of M1.0 and above have a large effect on space weather, they are known as large flares. The relationship between solar flares and Coronal Mass Ejections (CMEs) is of significant importance in solar research. Statistical analysis reveals that the likelihood of flares being associated with CMEs tends to rise as the flare's strength increases. Typically, the most formidable X-class flares are almost invariably accompanied by a CME event. Nevertheless, it's worth noting that reported percentages may vary depending on factors such as the solar cycle stage and the specific instrument or detection method employed for observations [59]. A solar event characterized by the occurrence of both a flare and a Coronal Mass Ejection (CME) is commonly referred to as an "eruptive" event. Conversely, when a flare occurs without an associated CME, it is termed an "enclosed" flare. Solar researchers typically employ the term "solar flare" to encompass both flares that are accompanied by CMEs and those that are not. flares and CMEs are aspects of solar activity that typically arise from magnetically active regions of strong, extensive, and often complex magnetic structures. The near-Earth space can be affected by flares and CMEs, and these effects can last for minutes, hours, and days.

[47] showed a connection between small coronal mass ejections and the evolution of their magnetic fluxes. Enhanced X-ray and Extreme Ultraviolet (EUV) radiation can lead to variations in electron density across various ionospheric altitudes. These fluctuations have a disruptive impact on radio communications. Moreover, the subsequent expansion of the Earth's atmosphere at higher altitudes results in increased atmospheric drag, which affects the orbital trajectories of low-altitude satellites. Space instrumentation can experience interference from both direct electromagnetic radiation and high-energy particles that get accelerated by Coronal Mass Ejection (CME) fronts. This phenomenon can impact the proper functioning of instruments in space. These effects can seriously damage the infrastructure, and disrupt communications, navigation systems and, power grids [15]. The origin of the stationary ridges and their eruptions related to CMEs have not yet been precisely determined. Vortex structures and countercurrents have now been seriously considered. The currents are a good representation of the magnetic field line of force, but the details are unknown. A large-scale vortex is observed in the high-latitude ridge observed on 13-14 November 2011, prior to its eruption. Using a Fourier local correlation tracking algorithm combined with a three-dimensional analysis of counter-radial flows with vortices in filaments with the dominant downward motion of plasma bubbles or plasmoids prior to prominent eruption is observed, [57]. A large-scale vortex structure was analyzed in detail, which shows a possible three-dimensional behavior. For the first time, synthetic stereograms were produced to show three-dimensional behavior. The Hα bulge, often observed on the solar limb, is intricately enveloped within a complex coronal temperature structure. This structure exhibits pronounced eddy motions within the chromospheric temperature plasma. Remarkably, this plasma remains suspended and constrained by the magnetic field up to half a day prior to its eventual eruption. Using the AIA images, the 3D surrounds of the

corona are visible, including the hot plasma at the bottom. Using the Yohkoh observations [78] observed a very strong X-ray jet forming. They introduced such a structure the active anemone zone. The occurrence of field line reconnection and the destruction of the magnetic field naturally indicates the existence of the neutral point. [78] concluded, based on two-dimensional numerical simulations, that the cause of the large X-ray jet generation is magnetic reconnection. [38] introduced a conceptual model for the formation of solar jets within a magnetic configuration. In this model, the energy source driving the process of energy release is attributed to a small, rotational flux tube.

By examining the changes in the structure of the magnetic field, the dynamics of coronal loops can be understood. By observing the direction of movement of coronal rings along the stream, the mechanism of jet formation becomes possible. Coronal loops typically originate from slender magnetic flux tubes containing plasma that is denser or hotter compared to the surrounding environment.

Usually, the expansion of loops occurs at the base of the jets, and after breaking the loops, and then starting the jets [79]. [24] reported the eruption of a small filament at the base of the EUV jet. [68] observed spiral twist in a EUV polar jet based on observations by the twin STEREO spacecraft. They found that the jet body appeared to open up as it ascended and, suggested that the driving mechanism for initiating polar jets was magnetic torsion. [37] using the analysis of observations at different wavelengths of a large-scale event in the region of ARs showed that it leads to forming a white light jet. Both large and small CMEs, as well as mini-CMEs, have been consistently observed using the Extreme Ultraviolet Imager (EUVI) aboard the Solar Terrestrial Relations Observatory (STEREO). These events are often accompanied by characteristic dimming and wave-like brightenings in the solar corona. [7] analyzed images of the solar full disk on 26 April 2008 with STEREO in pass band 195 Åand 171Å, and determined the velocities of the large and small wave-like brightening about 221 km s^{-1} and 6 km s^{-1}, respectively.

The slow wind originates at much less than the typical radial distance (r=2.5R$\odot$) where the LASCO C2 coronal hidden disk completely covers the central and most voluminous region of the solar corona. Therefore, the sources of the solar wind are not imaged. Analysis of the corona on it and very close to the solar disk is used by EUV imagers. However, These observations reveal fluctuations in both temperature and plasma density. It's important to note that the concealed inner disk within the more recent COR1 coronagraphs of the STEREO mission has a substantially smaller size compared to 2.5R$\odot$. Considering that their effective spatial resolution and signal-to-noise ratio are very suitable for recording small plasma bubbles, they are used in FOV detection and linear polarization analysis. They were called local plasma density enhancements, which were inferred in W-L properties similar to those of LASCO C2 bubbles, but starting at 1.5R$\odot$ and at radial velocities higher than $50R\odot$.

It turns out that flares that create waves and other transient phenomena generate the solar wind. Although the SPIRIT telescope is on a complex near-Earth orbit observing solar activity, it cannot be claimed that slow wind sources have been detected with EUV or even SXR imagers. CORONAS-F, with its large FOV, showed that above active regions, EUV coronal rays are recorded up to distances of 2 to 3R$\odot$, illustrating plasma outflows. Theoretically, the cause of solar wind can be diamagnetic plasmoids. [54] showed that the sources of plasmoids result from reconnection near the surface. Detached "spikes" from the corona or giant spicules are formed away from reattachment. [38] applied this mechanism to CH to explain the jets and possibly the fast wind, i.e., coronal streamers were excluded from the study. [41] reported near-boundary observations of some scattered high-velocity ARs outflow that may play an essential role in the slow solar wind mass-driving process. The lower corona consists of numerous coronal loops. The plasma associated with these coronal

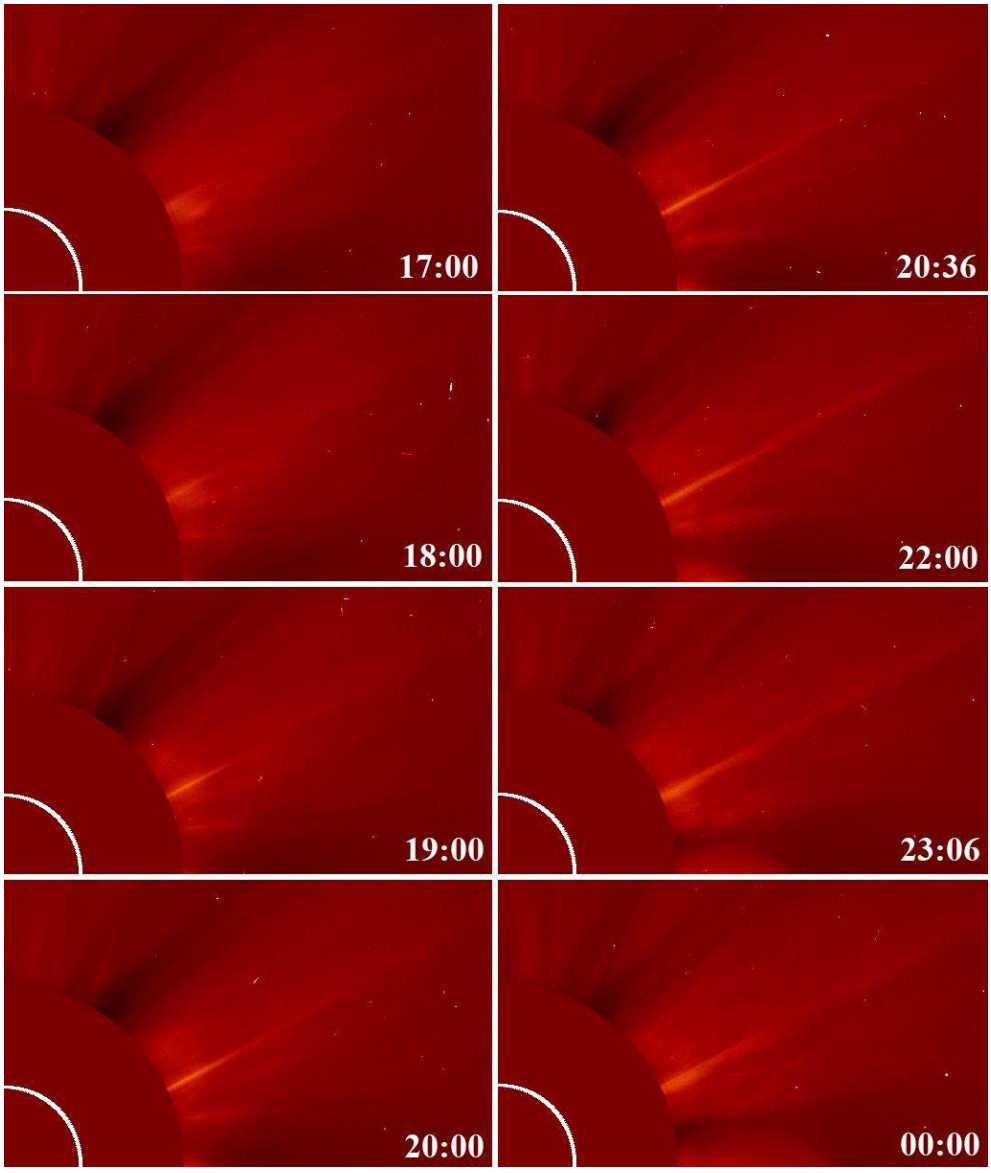

Figure 30: Displacement of the white-light linear ray like jet observed by the SOHO/LASCO-C2 coronagraph on 7 April 2011 [37].

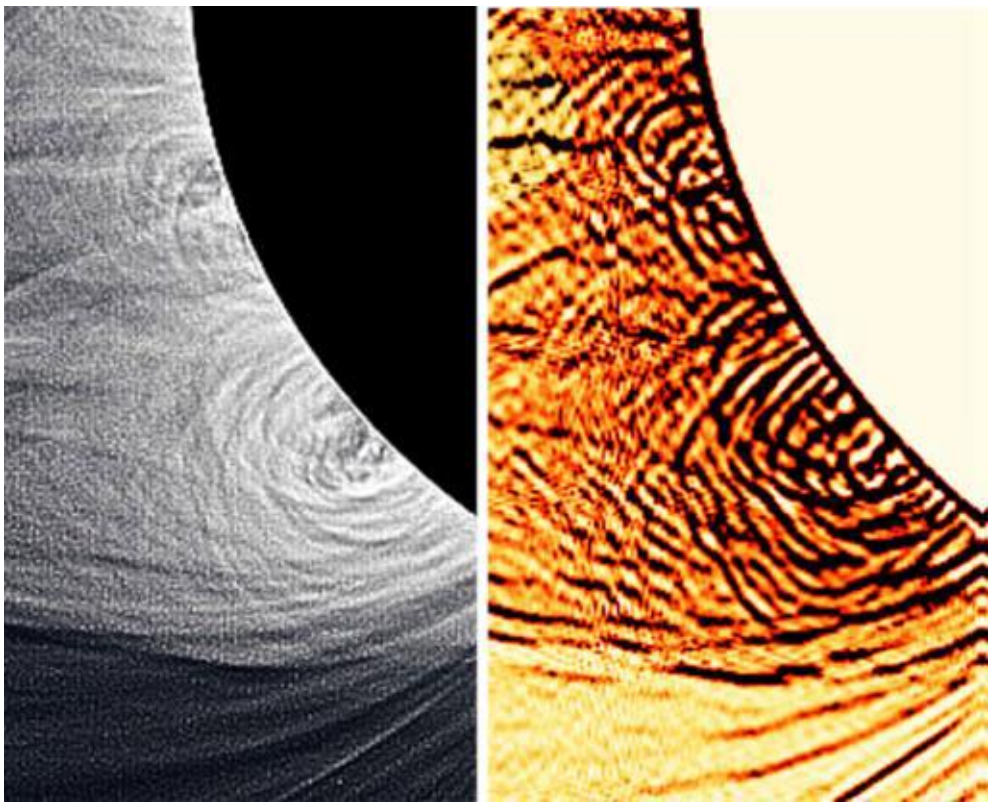

Figure 31: Highly processed WL eclipse image indicating the contour of loops and fine-scale details after removing the larger-scale gradients. The left image indicate after processing by the Madmax operator. the Madmax operator removes the photometric properties of the image [16].

loops in the magnetic fields is rooted in the layers of the photosphere. At higher altitudes, where the plasma can finally escape, observations are few.

[109] observed hot jets in the lower corona in SXR. Then, [38] observed hot jets in SXT of *Hinode*. In reference to [54], hot jets have been observed not only in Extreme Ultraviolet (EUV) lines but also in cooler chromospheric lines. This observation enables connections to be drawn between these hot jets and previous findings related to solar phenomena like waves, sprays, as well as macrospicules and spicules. These rapid eruption phenomena with the typical shape of the Eiffel Tower does not reach the critical radial distance to escape from it. Photometry of eclipse white light images (W-L) was studied by [95]. They showed a moving blob for the first time. They combined and aligned the SWAP images. These images were evaluated using a 20-hour sequence. SDO/AIA captured a magnetic reconnection event occurring in proximity to a high neutral point. This phenomenon was alternatively referred to as a magnetic plasmoid. The bubble's motion was quantified, revealing speeds of up to 12 km s^{-1}. The electron density of the isolated condensate (cloud or spot or plasmoid) was photometrically evaluated as 10 $^{8}cm^{-3}$ at r=1.7R$\odot$.

[58] have observed GCRs were characterized through images depicting individual nuclear reactions, commonly known as spallation events.

Such an event was captured on 29 November 2015, using a unique routine LASCO C3 space coronagraph image obtained during *the Solar and Heliospheric Observatory* (SoHO) mission in continuous observation at the L1 Lagrangian point. For the first time [58] observed the scaling signature of a GCR well detected outside the Earth's magnetosphere. Their resulting image consists of different linear "tracks" of different intensities leading to a single pixel. The coronal camera is detected by this location frame on the silicon CCD chip. During that period, there were no recorded occurrences of Coronal Mass Ejections (CMEs), and there was no discernible evidence of optical debris in the vicinity of the spacecraft. Over the course of two decades of uninterrupted observations conducted by the Solar and Heliospheric Observatory (SoHO), numerous instances of smaller Cosmic Ray (CR) events have been documented. [58] recorded the first crusting event from a CR, outside the Earth's magnetosphere. They evaluated these events in terms of energy, which is an acceptable galactic source. To begin, a total of 80 slitless visible eclipse flash spectra were combined and integrated. These flash spectra were compared with simultaneously obtained EUV SWAP/Proba2 174 Å images of ESA and AIA/SDO 171Å 193 Å 304 Å and 131 Å filtergrams. In a total solar eclipse, which is free of disturbing light, the junction of the corona and the corresponding cavity was investigated to study the prominence[16]. To investigate the electron density, an analysis was conducted on the visible continuum situated between the solar prominences, and increasing heating in the cavity region was shown [16], the photosphere to the chromosphere, and the prominence to the corona interface. These solar structures were witnessed during a total solar eclipse, and their characterization was reliant on the use of extreme ultraviolet (EUV) emission lines associated with both high and low temperatures. They analyzed a time series of rapidly changing coronal hole structures EUV data from SDO/AIA. They uncovered compelling evidence of events displaying acceleration characteristics within the 1.25 Mk line of Fe XII at 193 Å. They observed structures that were moving upwards with a speed of about 140 km s^{-1}. These phenomena can be understood as an upward-propagating wave when examined in the spectral lines 304 Å and 171 Å. Higher velocities are seen at 193 Å up to 1000 km s^{-1}. They found that this jump of cold He II plasma has a time delay of about 4 min in the lowest layer. At the highest level, it was more than 12 min late compared to the behavior of the hot 193 Å. The investigation involved the analysis of dynamics through the utilization of time slice diagrams. The outcomes of this analysis revealed that a substantial volume of material, ejected at high velocities, originates from beneath the columnar structure located at the base points.

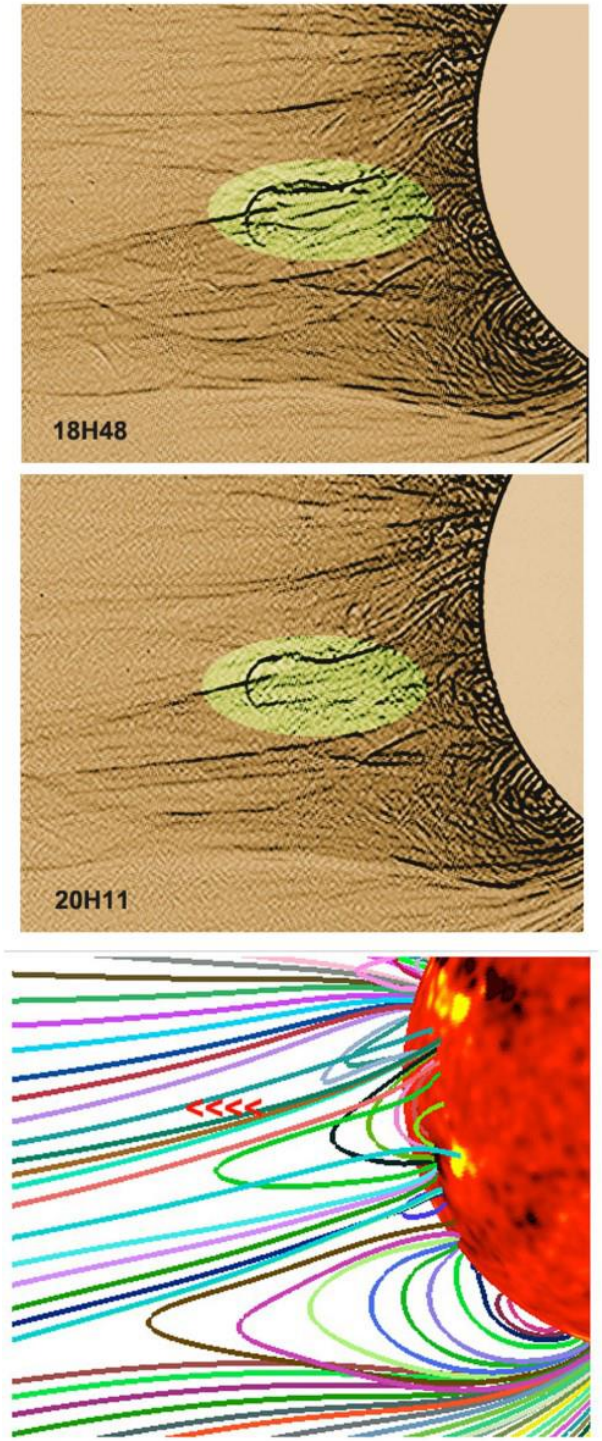

Figure 32: Top: high resolution W-L coronal images after processing by using the operator Madmax. The magnetic field topology is seen at best the coronal structure defined by small scale gradients supposed to represent [95].

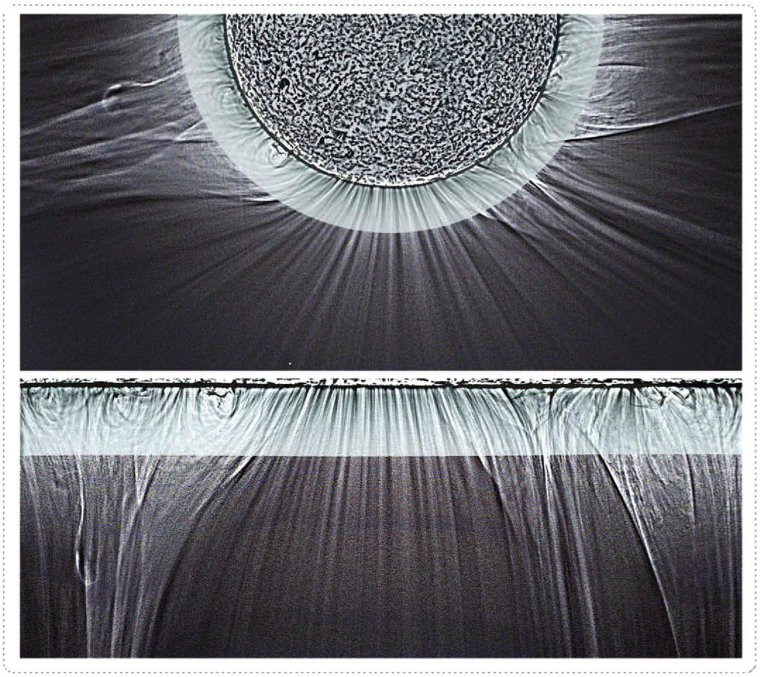

Figure 33: From top to bottom: composite white-light image of the 2010 July 11 total solar eclipse obtained at 20:14 UT on Easter Island in the southeastern Pacific Ocean and SDO/AIA observations in the EUV 171 Å line, and in polar coordinates. The AIA image obtained by summing and applying unsharp masking 150 frames with 12 s cadence from 20:00 to 20:30 UT [99].

They concluded that the plasma material released from a cylinder with reinforced walls has quasi-parallel edges.

In a study conducted by [104], the unusual thickness of the chromosphere situated above the solar poles' coronal holes (CH) was quantified using data from the Atmospheric Imaging Assembly (AIA) aboard the SDO. They collected and analyzed 13 years of data from 2010 to 2022, on the 15th of every month. They used light emitted from He II at a wavelength of 304 Å at about 50,000 Kelvin to probe the sun's north and south poles. According to their results, A peak increase in the number of sunspots around 2025 is anticipated, with a time delay of 2 to 5 years being attributed to the relationship between sunspot counts and solar activity in the coronal holes (CHs) situated at the solar poles. As a result, it is likely that the sunspot count during solar cycle 25 will exceed that of cycle 24, which was characterized by a notably low sunspot count. Furthermore, their findings suggest an inverse relationship between the thickness of the chromosphere and the magnetic activity cycle of the solar dynamo. Their analysis further underscores the inverse relationship between the thickness of the chromosphere and the magnetic activity cycle of the solar dynamo. Consequently, it is likely that solar cycle 25 will witness a higher number of sunspots compared to cycle 24, which was characterized by a lower sunspot count. This association between chromospheric thickness and solar dynamo magnetic activity is a notable finding of their study (see Figures 39-41).

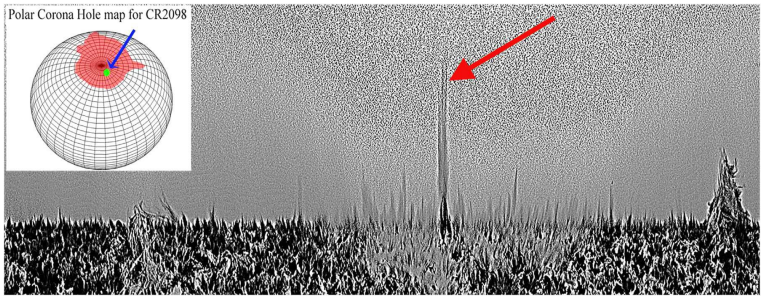

Figure 34: The north CH observations of 2010 July 10 in polar coordinates of the solar limb, in 304 Å after summing of 80 frames with a 12 s cadence(16 minutes between 14:28:52 and 14:44:40 UT, with unsharp masking). Intensities are in the logarithmic scale. The red arrows shows the longest jet near the center of the figure as a tornado [99].

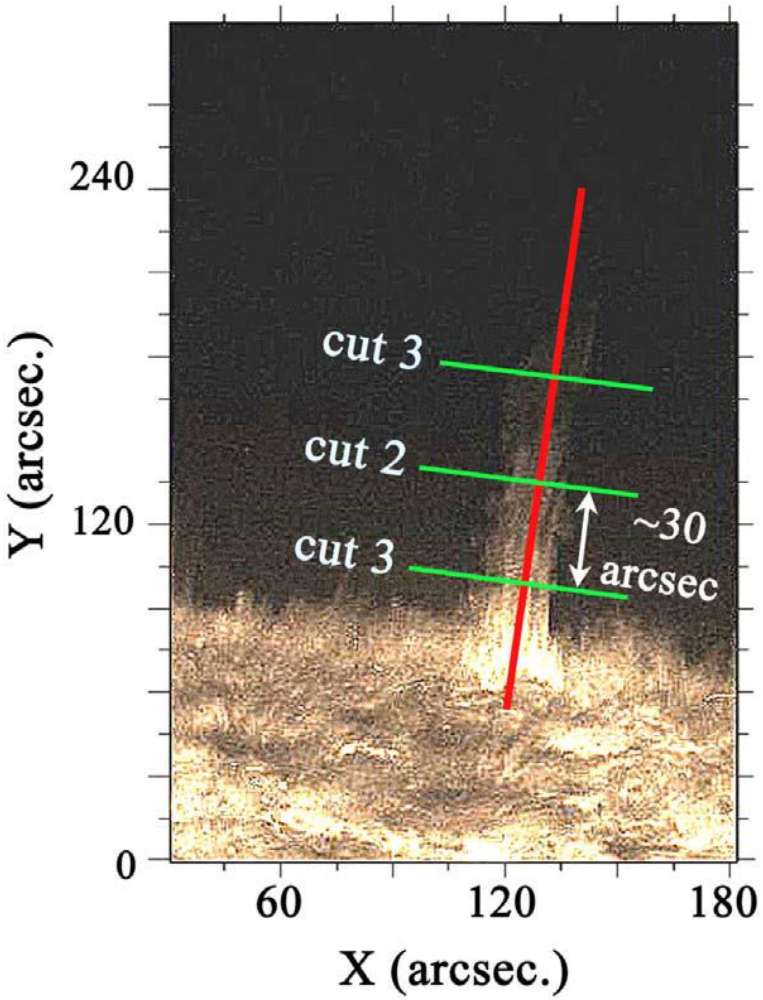

Figure 35: Example of snapshot in 304 Å line to show the main axis of the tornado with different cuts that are used to study the longitudinal motion [99].

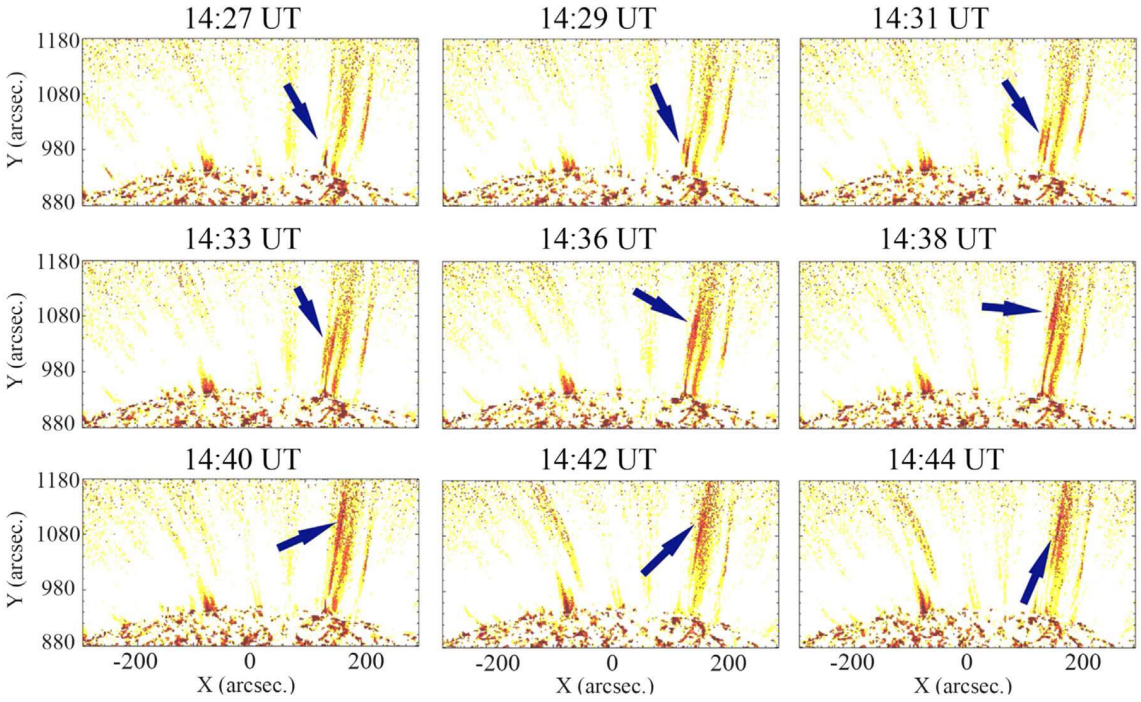

Figure 36: A typical coronal plume structure in AIA 171 Å, with time evolution of the acceleration inside [99].

5 Summary

This review aims to provide an overview of numerous studies conducted on fast solar jets and Coronal Mass Ejections (CMEs). Energetic events like these can have a profound impact on the space environment surrounding Earth, with effects manifesting over varying timescales, ranging from minutes to hours or even days. The heightened X-ray and Extreme Ultraviolet (EUV) emissions exert an immediate influence on electron density at different ionospheric altitudes, leading to disturbances in radio communications. Additionally, the subsequent expansion of the Earth's atmosphere results in increased drag on low-altitude satellites. Both the direct electromagnetic emissions and the energetic particles, whether accelerated in situ or by Coronal Mass Ejection (CME) fronts, pose significant risks to space-borne instrumentation and crew members. Furthermore, they can cause substantial damage to critical infrastructure, both in space and on the ground. This includes the disruption of communication networks, navigation systems, and power grids. There are two yet unresolved fundamental problems in Solar Physics: i/ heating of the solar corona and chromosphere, and ii/ origin of the solar wind. Both are related to the practical issue of Space Weather but also, the fundamental problem met in many fields of space physics and Astrophysics. The dissipation of the free energy of the magnetic field and its consequences. In addressing these challenges, it is imperative to engage in the analysis of extremely fine-scale dynamic phenomena. This is timely because some of the new space missions brought many of data concerning phenomena like macro-spicules and X-ray jets. The former problem of chromospheric "cool" spicules, believed to explain the plasma storage in the corona, is now completely renewed and can be more extensively analyzed. New diagnostics should also be considered to understand the processes inside the extended radial direction TR where

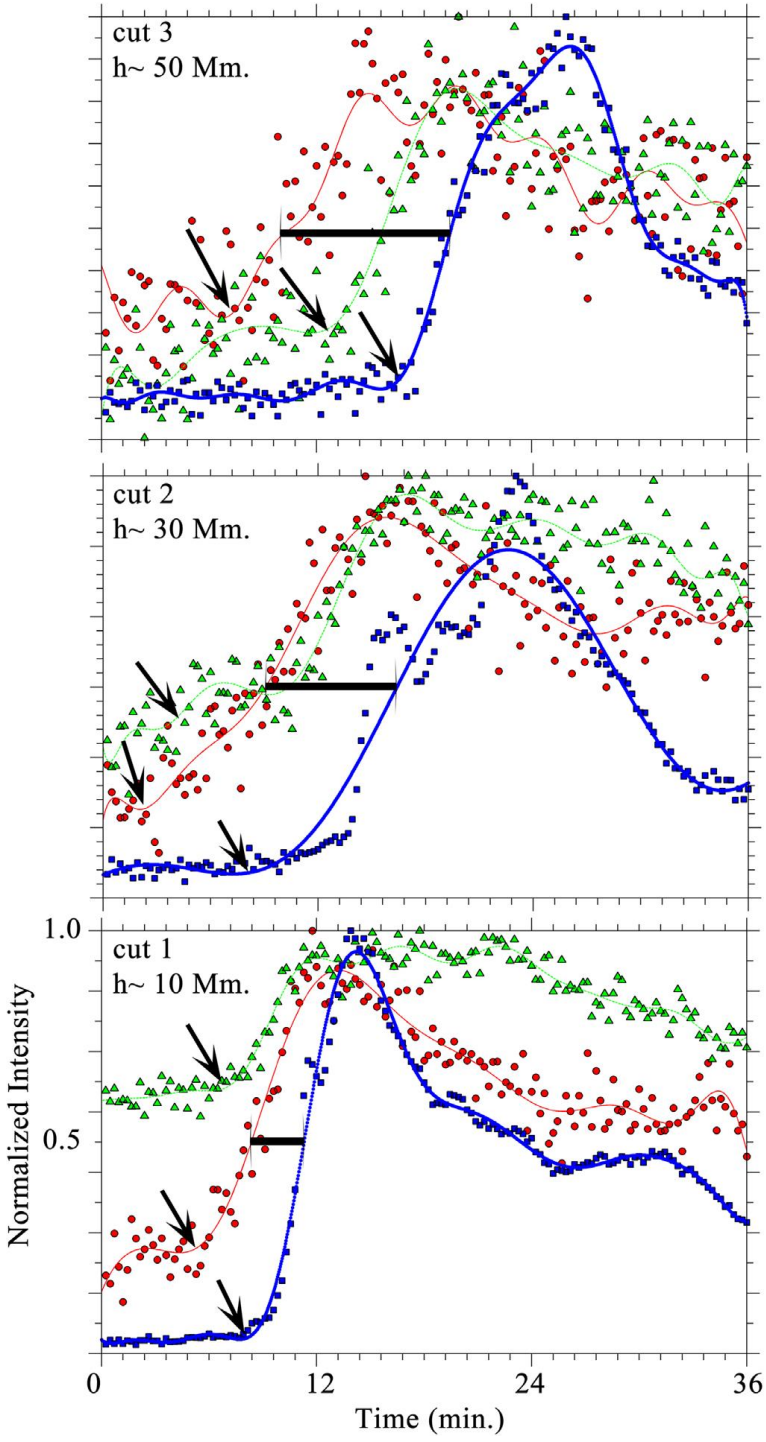

Figure 37: Time intensity variations along the three lines along the jet(indicated in Figure 35). The red dots, green triangles, and blue squares are for 193 Å, 171 Å, 304 Å respectively. The beginning phase of the sharp ascent of fitting intensities for different lines is indicated by black arrows. Time difference of the ejection in the TR (304 Å) and hot coronal line (193 Å)is shown by the black horizontal lines [99].

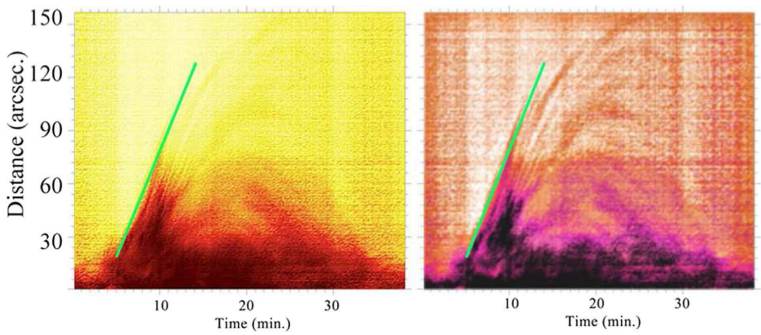

Figure 38: Time slice of intensity of the dynamical part of the jet. The width is 6 arcsec in 304 Å. The time slice obtained in the perpendicular direction of the jet main axis of the event shown in Figure 35 with a red line. Left: original display. The right panel obtained after using an unsharp masking filter. Plasma clouds following a quasi-parabolic path in time–distance diagram after 15 minutes is showed. It is seen the slope of the line is about 140 km s^{-1} [99].

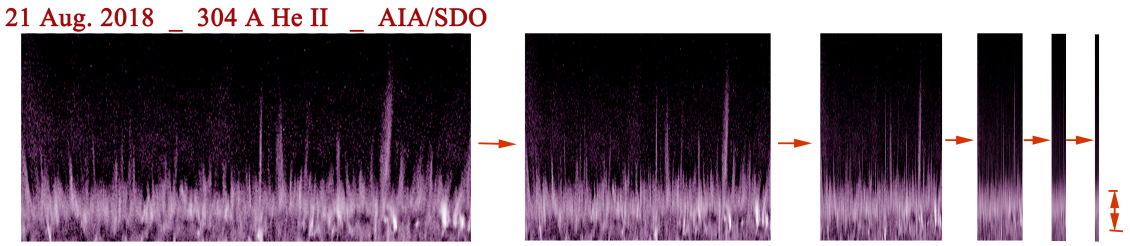

Figure 39: From left to right indicates time slices along the radial distance. This method applies by summing and averaging images to measure the width of the abnormal solar polar region on 21 August 2018 in 304 Å (50,000 K) [104].

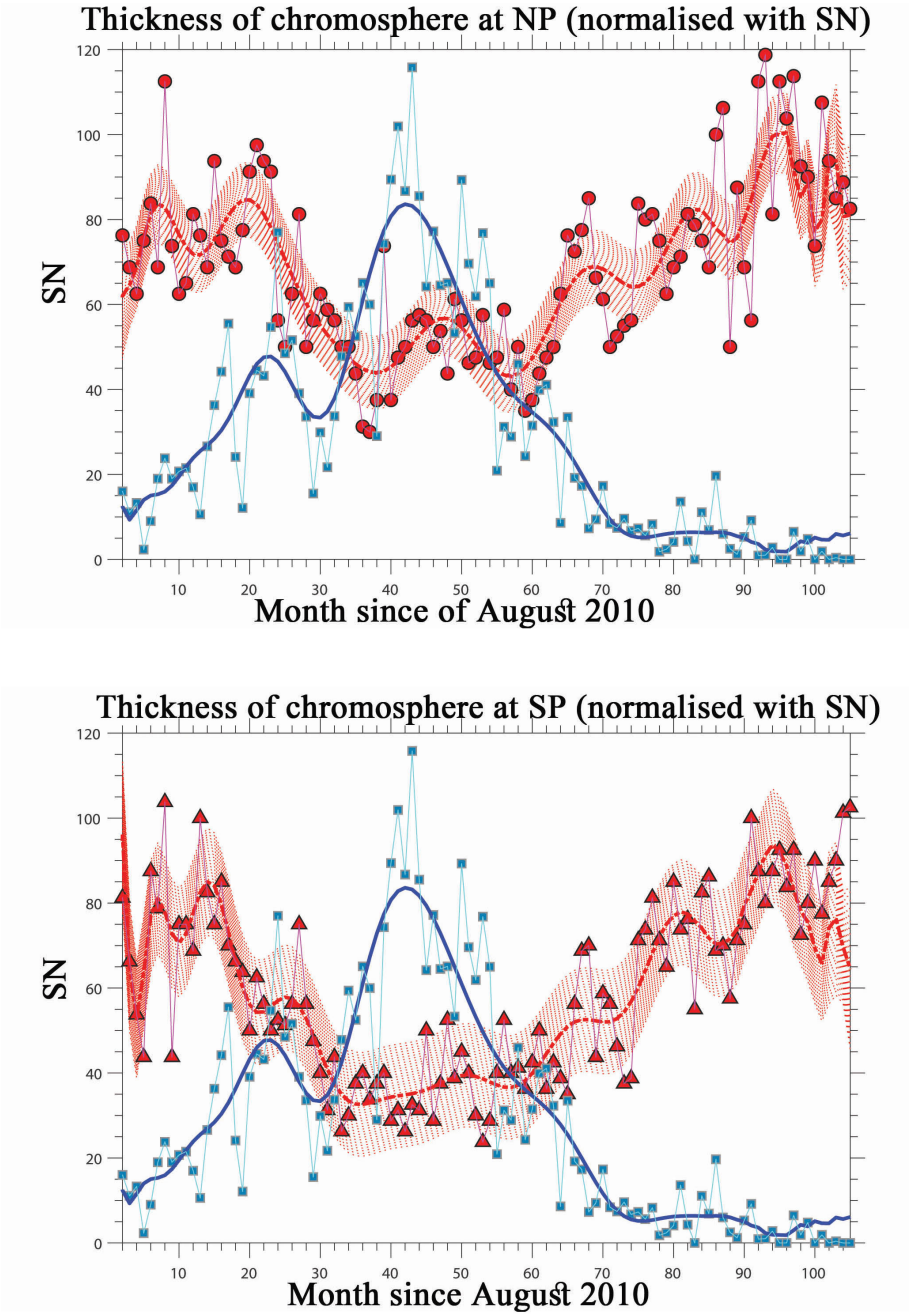

Figure 40: Variation of the number of sunspots and thickness of the chromosphere in the north pole (top) and the south pole of the Sun (bottom) [104].

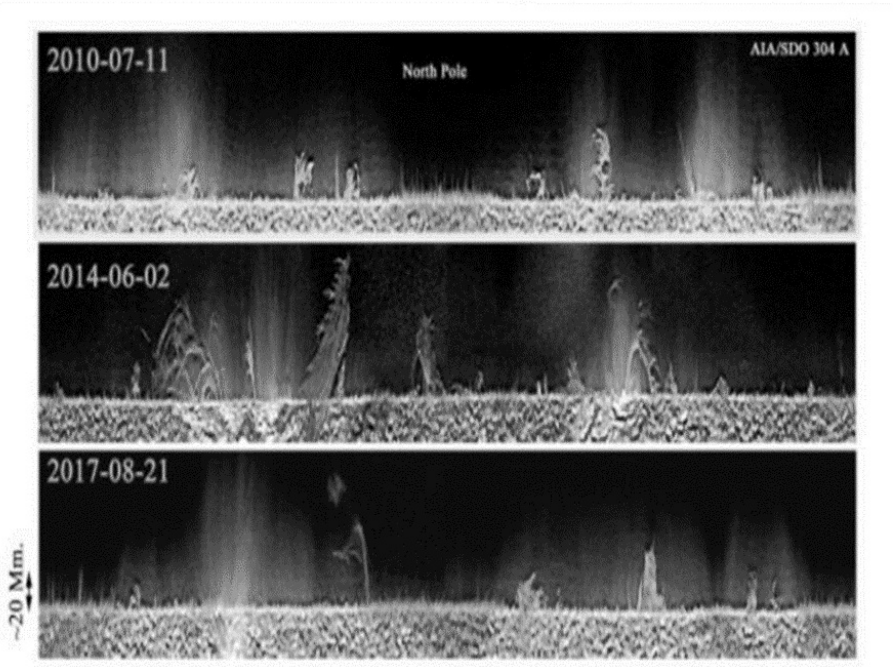

Figure 41: Radial time slices of solar disk in the three data in the 24 solar cycle. In the minimum and maximum activity it is seen an increase and decrease in the thickness of the chromosphere at the poles, respectively [104].

magnetic energy is released. Questions related to the interpretation of reported observations of apparent oscillations and waves were discussed, with emphasis on overlapping (superposition) effects to evaluate errors and possibly, explain observations, without implying any oscillations. We also note that this paper ought to be used for better understanding global space weather. Upon the arrival of Coronal Mass Ejections (CMEs) in the magnetosphere, their interactions with the Earth's magnetic field can instigate space weather phenomena. The relationships elucidated in these findings have the potential to be invaluable in predicting space weather events when they are observed.

Authors' Contributions

All authors have the same contribution.

Data Availability

No data available.

Conflicts of Interest

The authors declare that there is no conflict of interest.

Ethical Considerations

The authors have diligently addressed ethical concerns, such as informed consent, plagiarism, data fabrication, misconduct, falsification, double publication, redundancy, submission, and other related matters.

Funding

This research did not receive any grant from funding agencies in the public, commercial, or nonprofit sectors.

References

[1] Ajabshirizadeh, A., Tavabi, E., & Koutchmy, S. 2008, New Astron., 13, 93.

[2] Ajabshirizadeh, A., Tavabi, & E., Koutchmy, S. 2009, A&SS, 319, 31.

[3] Ajabshirizadeh, A., Koutchmy, S., & Tavabi, E. 2008, Resolution Effect in the Solar Spicules Oscillations, 12th European Solar Physics Meeting, Freiburg, Germany, held September, ESPM, 12, 44.

[4] Ajabshirizadeh, A., Tavabi, E., & Koutchmy, S. 2008, "Magneto-Acoustic Wave (KINK) Oscillations In Solar Spicules" First Middle East and Africa IAU-Regional Meeting Proceedings MEARIM, 1, 109.

[5] Almeida, J. S., Bonet, J. A., Viticchié, B., & Moro, D. D. 2010, ApJL, 715, L26.

[6] Alipour, N., & Safari, H. 2015, ApJ, 807, 175.

[7] Alipour, N., & Safari, H. 2019, IJPR. 12, 29.

[8] Alipour, N., Safari, H., Verbeeck, C., Berghmans, D., & et al. 2022, A&A, 663, 12.

[9] Alipour, N., Safari, H., & Innes, D. 2012, ApJ, 746, 8.

[10] Abramenko, V., Yurchyshyn, V., Goode, P., Kilcik, A. 2010, ApJ, 725, L101.

[11] Amirkhanlou, E., Tavabi, E., & Zeighami, S. 2018, JESP, 44, 674.

[12] Athay, R. G. 1961, ApJ, 134, 756.

[13] Athay, R. G. ApJ, 66, 278.

[14] Athay, R. G. 1974, Radiation Pressure in Stellar Atmospheres with Application to Solar Spicules, Cambridge University Press.

[15] Balasis, G., Papadimitriou, C., & Boutsi, A. Z. 2019, Ionospheric response to solar and interplanetary disturbances: a Swarm perspective. Philosophical Transactions of the Royal Society of London Series A, 377, 20180098.

[16] Bazin, C., Koutchmy, S., & Tavabi, E. 2012, Prominence-cavity regions observed in 2010 eclipse flash spectra and SWAP images, EAS, 55, 185B.

[17] Beckers, J. M. 1968, SoPh, 3, 367.

[18] Berger, T. E., Lofdahl, M. G., Shine, R. A., & Title, A. M. 1998, ApJ, 506, 439.

[19] Brueckner, G. E., & Bartoe, J. D. F. 1983, ApJ. 272, 329.

[20] Brueckner, G. E. 1980, in Highlights in Astron. Reidel Publ. 5, 557.

[21] Brueckner, G. E. 1981, Space Sci. Rev., 29, 407.

[22] Bohlin, J. D., Vogel, S. N., Purcell, J. D., Sheeley, N. R., Jr., Tousey, R., & Vanhoosier, M. E. 1975, ApJ. 197, L133.

[23] Beckers, J. M. 1966, ApJ, 71, 155.

[24] Chae, J. Qiu, J. Wang, H., & Goode, P. R. 1999, ApJL. 513, L75.

[25] Cheng, Q. Q., Ulmschneider, P., & Korevaar, P. 1991, Mechanisms of Chromospheric and Coronal Heating, Proceedings of the International Conference, New York, 350.

[26] Chen, P. F. 2011, Coronal Mass Ejections: Models and Their Observational Basis. Living Reviews in Solar Physics, 8.

[27] Cirtain, J. W., & et al. 2007, Science, 318, 1580.

[28] Daw, A., DeLuca, E. E., & Golub, L. 1995, ApJ, 453, 929.

[29] Defouw, R. J. 1976, ApJ, 209, 266.

[30] de la Cruz Rodríguez, J., Pontieu, B. D., Carlsson, M., & Van der Voort, L. H. M. R. 2013, ApJ, 764, L11.

[31] De Pontieu, B., Carlsson, M., Rouppe van der Voort, L. H. M., & et al. 2012, ApJ, 752, L12.

[32] De Pontieu, B., Erdélyi, R., & James, S. P. 2004, Nature, 430, 536.

[33] Dere, K. P., Bartoe, J. D. F., & Brueckner, G. E. 1983, ApJ, 2, 267.

[34] Dere, K. P. Bartoe, J. D., & Brueckner, G. E. 1989, SoPh. 123, 41.

[35] de Wijn, A. G., Lites, B. W., Berger, T. E., Frank, Z. A., Tarbell, T. D., & Ishikawa, R. 2008, ApJ, 684, 1469.

[36] Dunn, R. B., Zirker, J. B. 1973, SoPh, 33, 281.

[37] Filippov, B., Koutchmy, S., & Tavabi, E. 2013, SoPh. 286, 143.

[38] Filippov, B., Koutchmy, S., & Golub, L. 2009, Geomagnetism and Aeronomy, 49, 1109.

[39] Golub, L., Krieger, A. S., & Vaiana, G. S., 1975, SoPh., 42, 131.

[40] Georgakilas, A. A., Koutchmy, S., & Alissandrakis, C. F. 1999, A&A, 341, 610.

[41] Guo, L.-J., Tian, H., & He, J.-S. 2010, ApJ, 10, 1307.

[42] Haerendel, G. 1992, Nature, 360, 241.

[43] Moore, R. L., Cirtain, J. W., Sterling, A. C., & Falconer, D. A. 2010, ApJ, 720, 757.

[44] Halain, J. P., Berghmans, D., Defise, J. M., Renotte, E., Thibert, T., Mazy, E., & et al. 2010, Space Telescopes and Instrumentation, Ultraviolet to Gamma Ray, Proceedings of the SPIE, 7732, 77320P.

[45] Harrison, R. A., Bryans, P., & Bingham, R. 2001, A&A, 379, 324.

[46] Hofmeister, U., Dominik, H., & Stephan, G. 2019, Veronig, Astrid Temmer, Manuela, A&A.

[47] Honarbakhsh, L., Alipour, N., & Safari, H. 2016, SoPh. 291, 941.

[48] Innes, D. E., Inhester, B., Axford, W. I., & Wilhelm, K. 1997, Nature, 386, 811.

[49] Jafarzadeh, S., Solanki, S. K., Stangalini, M., Steiner, O., Cameron, R. H., & Danilovic, S. 2017, ApJ, 229, 10.

[50] Javaherian, M., Safari, H., Dadashi, N., & Aschwanden, M., 2017, SoPh, 292, 15.

[51] Jess, D. B., Mathioudakis, M., Christian, D. J., Crockett, P. J., & Keenan F. P. 2010.

[52] Kayshap, P., & Dwivedi, B. N. 2017, SoPh, 292, 108.

[53] Koutchmy, S., & Stellmacher, G. 1976, SoPh., 49, 253.

[54] Koutchmy, S., & Loucif, M. L. 1991, in: Ulmschneider P., Priest E. R., Ros-ner R. (eds.), Springer-Verlag, 152.

[55] Koutchmy, S., Hara, H., Suematsu, Y., Reardon, K. 1997, A&A, 320, L33.

[56] Koutchmy, S., Hara, H., Shibata, K., Suematsu, Y., & Reardon, K. 1998, In: Watanabe, T., Kosugi, T., Sterling, A. C.

[57] Koutchmy, S., Filippov, B., Tavabi, E., Bazin, C., & Weiller, S. 2013, Nature of Prominences and their role in Space Weather Proceedings IAU Symposium.

[58] Koutchmy, S., Tavabi, E., & Urtado, O. 2018, MNRAS., 478.

[59] Lamy, P. L., Floyd, O., Boclet, B., Wojak, J., Gilardy, H. & Barlyaeva, T. 2019, Space Sci. Rev., 215, 39.

[60] Lites, B. W., Rutten, R. J., & Kalkofen, W. 1993, Apj, 414, 345.

[61] Lites, B. W., Thomas, J. H., Bogdan, T. J., & Cally, P. S. 1998, ApJ, 497, 464.

[62] Madjarska, M. S., Doyle, J. G., Teriaca, L., & Banerjee, D. 2003, A&A, 398, 775.

[63] Moore, R. L., Tang, F., Bohlin, J. D., & Golub, L. 1977, ApJ. 218, 286.

[64] Muller, R., Dollfus, A., Montagne, M., Moity, J., & Vigneau, J. 2000, A&A, 359, 373.

[65] Parmenter, B. C. 1966, Publications of the Astronomical Society of the Pacific, 78, 463.

[66] Pasachoff, J. M., Jacobson, W. A., & Sterling, A. C., 2009, SoPh. 260, 59.

[67] Papushev, P. G., & Salakhutdinov, R. T. 1994, ApJ, 136, 250.

[68] Patsourakos, S., Pariat, E., Vourlidas, A., Antiochos, S. K., & Wuelser, J. P. 2008, ApJ, 680, L73.

[69] Roberts, W. O. 1945, ApJ, 101, 136.

[70] Rubio, L. B., & Suarez, D. O. 2019, Living Reviews in Solar Physics, 16, 1.

[71] Roudier, T., Rieutord, M., Brito, D., Rincon, F., Malherbe, J. M., Meunier, N., Berger, T., & Frank, Z. 2009, A&A, 495, 945. 945

[72] Rush, J. H., & Roberts, W. O. 1953, ApJ, 58, 226.

[73] Sadeghi, R., & Tavabi, E. 2022, ApJ, 938, 945.

[74] Sadeghi, R., & Tavabi, E. 2022, MNRAS, 512, 4164.

[75] Sheeley, N. R., & Golub L. 1979, SoPh, 63, 119.

[76] Sheeley, N. R. 1967, SoPh, 1, 171.

[77] Shibata, K., & Magara, T. 2011, Solar Flares: Magnetohydrodynamic Processes. Living Rev. Solar Phys., 8.

[78] Shibata, K., Nitta, N., Strong, K. T., Matsumoto, R., Yokoyama, T., Hirayama, T., Hudson, H., & Ogawara, Y. 1994, ApJL. 431, L51.

[79] Shimojo, M., Hashimoto, S., Shibata, K., Hirayama, T., Hudson, H. S., & Acton, L. 1996, Publ. Astron. Soc. Japan, 48, 123.

[80] Shimojo, M., Narukage, N., Kano, R., Sakao, T., Tsuneta, S., Shibasaki, K., & et al. 2007, Publ. Astron. Soc. Japan, 59, S625.

[81] Simon, G. W., & Leighton, R. B. 1964, ApJ, 140, 1120.

[82] Singh, K. A. P., Isobe, H., Nishida, K., & Shibata, K. 2012, ApJ, 760, 28.

[83] Snodgrass, H. B., & Ulrich, R. K. 1990, ApJ, 351, 309.

[84] Stangalini, M., Giannattasio, F., Moro, D. D., & Berrilli, F. 2012, A&A, 539, L4.

[85] Sterling, H. C. 2000, SoPh., 196, 79.

[86] Sterling, A. C., Harra, L. K., & Moore, R. L. 2010, ApJ, 722, 1644.

[87] Suematsu, Y., Ichimoto, K., Katsukawa, Y., Shimizu, T., Okamoto, T., Tsuneta, S., Tarbell, T., & Shine, R. A. 2008, Astron. Soc. Pac., 397, 27.

[88] Tavabi, E., Koutchmy, S., & Ajabshirzadeh, A. 2011, New Astron., 16, 296.

[89] Tavabi, E., Koutchmy, S., & Ajabshirizadeh, A. 2011, Adv. Space Res., 47.

[90] Tavabi, E. 2012, J. Modern Physics, 3, 11, 1786.

[91] Tavabi, E., Koutchmy, S., & Ajabshirizadeh, A. 2013, SoPh., 283, 187.

[92] Tavabi, E., & Koutchmy, S. 2014, Ap&SS, 352, 7T.

[93] Tavabi, E. 2014, Ap&SS, 350, 489.

[94] Tavabi, E. 2014, Ap&SS, 352, 43.

[95] Tavabi, E., Koutchmy, S., & Bazin, C. 2018, SoPh., 293, 42T.

[96] Tavabi, E., Ajabshirizadeh, A., Ahangarzadeh Maralani, A. R., & Zeighami, S. 2015, J. ApA, 41, 18.

[97] Tavabi, E., Koutchmy, S., Ajabshirizadeh, A., Ahangarzadeh Maralani, A. R., & Zeighami, S. 2015, A&A, 573, 7.

[98] Tavabi, E., Koutchmy, S., & Golub, L. 2015, SoPh., 290, 2871.

[99] Tavabi, E., Koutchmy, S., & Golub, L. 2018, ApJ, 866, 35.

[100] Tavabi, E. 2018, MNRAS, 476, 868.

[101] Tavabi, E., & Koutchmy, S. 2019, ApJ, 883, 41.

[102] Tavabi, E., Zeighami, S., & Heydari, M. 2022, SoPh., 297, 76.

[103] Tavabi, E., & Sadeghi, R. 2022, JESP, 48, 749.

[104] Tavabi, E., Rajabi, M., & Zeighami, S. 2022, IJAA.

[105] Tavabi, E., & Zeighami, S. 2022, IJAA.

[106] Tsiropoula, G., Tziotziou, K., Kontogiannis, I., & et al. 2012, Space Sci. Rev., 169, 181.

[107] Utz Hanslmeier, A., Mostl, C., Muller, R., Veronig, A., & Muthsam, H. 2009, A&A, 498, 289.

[108] Yokoyama, T., & Shibata K. 1995, Nature, 375, 42.

[109] Yokoyama, T., & Shibata, K. 1996, PASJ, 48, 353.

[110] Wang, Y. M., & Sheeley, N. R. 2002, ApJ, 575, 542.

[111] Webb, D. F., & Howard, T. A. 2012, Coronal Mass Ejections: Observations, Living Reviews in Solar Physics, 9.

[112] Wulser, J.-P., Lemen, J. R., Tarbell, T. D., Wolfson, C. J., Cannon, J. C., Brock, A., & Carpenter, B. A., 2004, Telescopes and Instrumentation for Solar Astrophysics, Proc. SPIE 5171, 111.

[113] Xiong, J., Yang, Y., Jin, C., Ji, K., Feng, S., Wang, F., Deng, H., & Hu, Y. 2017, ApJ.

[114] Yamauchi, Y., Wang, H., Jiang, Y., Schwandron, N., & Moore, R. L. 2005, ApJ, 629, 572.

[115] Zeighami, S., Ahangarzadeh Maralani, A. R., Tavabi, E., & Ajabshirizadeh, A. 2016, SoPh., 291, 847.

[116] Zeighami, S., Tavabi, E., & Amirkhanlou, E. 2020, JApA., 41, 18Z.

[117] Zeighami, S., & Tavabi, E. 2021, JESP, 44, 671.

[118] Zeighami, S., & Tavabi, E. 2021, IJAA.

[119] Zeighami, S., Tavabi, E., & Ajabshirizadeh, A. 2023, JESP.

[120] Zirker, J. B. 1962, ApJ, 135, 515.

[121] Zirker, J. B. 1962, ApJ, 136, 250.